Mechanics Research Communications 156 (2026) 104754

Contents lists available at ScienceDirect

Mechanics Research Communications

journal homepage: www.elsevier.com/locate/mechrescom

An asymptotic strain-based formulation for isotropic damage with unilateral effects in thin adhesive layers[☆]

Michele Serpilli [a], Raffaella Rizzoni [b,*], Hélène Welemane [c], Frédéric Lebon [d]

[a] Polytechnic University of Marche Department of Civil and Construction Engineering and Architecture, Italy
[b] University of Ferrara Department of Engineering, Italy
[c] Univ Toulouse, UTTOP, INSA Toulouse, LMDC, Tarbes, France
[d] Aix-Marseille University, France

ARTICLE INFO

Keywords:
Asymptotic interface model
Unilateral damage
Adhesive joints
Tension–compression asymmetry
Damage evolution

ABSTRACT

The mechanical response of adhesive joints is strongly influenced by damage mechanisms exhibiting tension–compression asymmetry, driven by the opening and closure of microcracks. In this work, a strain-based formulation for isotropic damage with unilateral effects is employed. The damage model is developed within a thermodynamically consistent framework with internal variables. Moreover, it provides a physically motivated representation of microcrack-induced degradation, incorporating recovery effects associated with crack closure and allowing for distinct responses under tensile and compressive loading conditions. The formulation is applied to a thin adhesive layer connecting two elastic adherents, and an asymptotic analysis is performed to derive an effective mechanical description of the damage evolution of the bonded joint. The predictive capabilities of the proposed approach are assessed through the analysis of a uniaxial test on a butt joint. The results highlight the role of unilateral effects in governing the global response, particularly in terms of stiffness degradation, damage evolution and the difference between tensile and compressive regimes.

1. Introduction

The reliable prediction of damage and failure in bonded assemblies remains a central issue in structural engineering. Structural adhesives are widely employed to join metallic, composite and hybrid components, offering advantages such as stress redistribution, weight reduction and improved fatigue resistance compared to traditional mechanical fastening. In many applications, the adhesive layer plays a decisive mechanical role: its degradation governs stiffness loss, load transfer capability and, ultimately, structural integrity.

From a mechanical point of view, structural adhesives exhibit a markedly different response in tension and compression. In tension, microdefects such as voids, inclusions and microcracks tend to open and propagate, leading to stiffness degradation, brittle-like failure, and eventual decohesion. Under compression, however, the same microdefects may close, partially restoring stiffness and delaying damage progression. This phenomenon results in an intrinsic unilateral behavior, characterized by asymmetric constitutive responses under positive and negative normal strains. Such tension–compression asymmetry can occur in quasi-brittle materials such as concrete [1,2], in ductile materials such as metals [3,4], in polymers [5], and also composite adhesive joints [6,7]. Continuum Damage Mechanics (CDM) provides a rigorous thermodynamic setting for modeling progressive stiffness degradation induced by distributed microdefects [8–10]. Within this framework, the material response is derived from a free energy potential coupled with an appropriate dissipation pseudo-potential, ensuring consistency with the second law of thermodynamics. To account for unilateral effects, several strategies have been proposed in the literature: for instance, the spectral decomposition [11], where the strain tensor is split according to the sign of its principal values, allowing the elastic energy associated with positive and negative eigenvalues to be treated separately; the volumetric–deviatoric decomposition [12,13], in which only the deviatoric part of the strain energy contributes to the damage process; the star-convex model [14], where the remaining elastic energy density depends exclusively on the negative trace of the strain tensor. A comprehensive discussion of more advanced phase-field formulations incorporating tension–compression asymmetry can be found in [15].

As pointed out by many authors (see, e.g., [16–18]), the account of the unilateral effects often leads to serious inconsistencies in macroscopic formulations. The approach introduced by Welemane and

[☆] This article is part of a Special issue entitled: ‘Multi. Asympt. Meth. Solid Mech.’ published in Mechanics Research Communications.

* Corresponding author.
E-mail address: raffaella.rizzoni@unife.it (R. Rizzoni).

https://doi.org/10.1016/j.mechrescom.2026.104754
Received 24 April 2026; Received in revised form 3 June 2026; Accepted 16 June 2026
Available online 25 June 2026

Cormery [19–21] provides a consistent and physically motivated continuum description of microcrack opening–closure effects, within the framework of thermodynamics with internal variables. The model is characterized by a damage representation based on the distribution density of microcracks and formulated through fabric tensors. It incorporates a recovery condition associated with microcracks closure, derived from micromechanical considerations, and avoids the use of spectral decompositions, while the damage evolution law follows the standard thermodynamic arguments. In addition, the formulation possesses a modular structure, allowing it to be extended to different levels of damage induced anisotropy, see [19,22].

When adhesive joints are analyzed at the structural scale, interface models, most notably Cohesive Zone Models (CZMs), are frequently adopted. In these formulations, the thin adhesive layer is replaced by a zero-thickness surface endowed with a traction–separation law, see for example [23–27] and the references therein. Although such models are computationally efficient and capable of reproducing complex nonlinear phenomena, their constitutive parameters are often phenomenological and not directly linked to the physical properties or microstructure of the actual adhesive layer. This lack of a rigorous connection between bulk damage mechanisms and interface laws limits the predictive capability of cohesive approaches, particularly when tension–compression asymmetry and microcrack closure effects are involved. Damage processes in interphases have also been addressed in homogenization approaches. For instance, Nazarenko et al. [28] proposed a statistical damage model for spring-layer interfaces in random particular composites. In that model, the spring stiffness is reduced according to the local fraction of damaged interface, which is estimated through a Weibull distribution of local interfacial strengths. The Weibull parameters provide a phenomenological statistical description of damage activation.

In the context of thin adhesive layer, a consistent alternative consists in deriving interface models from a three-dimensional damaging interphase by means of asymptotic techniques. Starting from a thin adhesive layer, whose thickness depends on a small parameter ε, one can apply asymptotic expansion method with respect to ε, transforming the original three-dimensional equilibrium problem into an effective imperfect interface model. In this way, the transmission conditions at the interface inherit the constitutive features of the bulk adhesive, including damage evolution and unilateral effects. The asymptotic techniques have been applied in different contexts such as linear [29–32] and nonlinear elastic interface models [33,34], contact of rough surfaces [35], initially isotropic [36,37] or anisotropic [38] damaging materials, taking into account also unilateral effects [39], and multiphysics theories [40,41].

The objective of the present work is to develop a mechanically consistent formulation for the description of damage evolution in thin adhesive layers exhibiting unilateral effects. Starting from a strain-based isotropic damage model capable of representing microcrack opening and closure mechanisms, following and adapting the approaches developed in [19–21], the study aims to derive a structural description of the interface behavior suitable for bonded assemblies. In contrast with statistical damage descriptions based on phenomenological strength distributions, the present formulation obtains the interface response from a thermodynamically consistent damage model and from the asymptotic limit of a thin adhesive layer.

To illustrate the predictive capabilities of the proposed approach, the model is applied to the analysis of a bonded structure subjected to uniaxial test, under hard (displacement-controlled) and soft (force-controlled) loading device conditions, respectively. In particular, the response of a butt joint is investigated, allowing the influence of unilateral damage effects on the global force–displacement behavior to be highlighted. The theoretical analysis allowed the characterization of different regimes (elastic, damage evolution and snap-back instabilities) and the associated activation thresholds, in terms of the constitutive material parameters. The numerical simulations provide insight into the evolution of damage under tensile and compressive regimes and demonstrate the relevance of the proposed formulation for the realistic modeling of adhesive joints.

The paper is organized as follows. Section 2 introduces the theoretical framework of the strain-based isotropic damage evolution model, with unilateral effects. Section 3 describes the asymptotic expansions procedure adopted to derive the effective limit models for the thin interphase and discusses the resulting formulations. Section 4 illustrates the predictive capabilities of the proposed approach through the analysis of a uniaxial test on a butt joint, highlighting the influence of unilateral damage effects on the structural response. Finally, Section 5 is devoted to the concluding remarks.

2. Theoretical framework of damage evolution

In this section, the isotropic version of the three-dimensional damage model is presented, considering the approach developed in [19–21]. The constitutive model outlined below aims to represent microcrack-induced degradation and the associated mechanical response of quasi-brittle materials under rate-independent, isothermal conditions and small deformations. The model considers a single dissipative mechanism, namely the initiation and propagation of non-interacting microcracks, and is grounded in a thermodynamically consistent damage framework. Micromechanically based assumptions are adopted to account for microcrack closure effects.

2.1. General formulation

In the sequel, Latin indices range in the set $\{1,2,3\}$, while Greek indices are taken in the set $\{1,2\}$, and the Einstein's summation convention is employed. The following notations are adopted: for all vectors $\mathbf{a} = (a_i)$ and $\mathbf{b} = (b_i)$, $(\mathbf{a}\otimes\mathbf{b})_{ij} := a_i b_j$, $(\mathbf{a}\odot\mathbf{b})_{ij} := \frac{1}{2}(a_i b_j + a_j b_i)$ and $\mathbf{a}^{\otimes i} := \mathbf{a}\otimes\mathbf{a}\ldots\otimes\mathbf{a}$, $i\in\mathbb{N}$, denote the dyadic, the symmetric diadic and the ith dyadic products, respectively. Thus, $\mathbf{a}^{\otimes 2} = \mathbf{a}\otimes\mathbf{a}$. Moreover, the same notation will be used for the vector and tensor scalar products, i.e., $\mathbf{a}\cdot\mathbf{b} := a_i b_i$ and $\mathbf{A}\cdot\mathbf{B} := A_{ij}B_{ij}$, for all vectors $\mathbf{a} = (a_i)$ and $\mathbf{b} = (b_i)$, and for all tensors $\mathbf{A} = (A_{ij})$, $\mathbf{B} = (B_{ij})$.

The damage scalar variable d, accounting for the isotropic part of the microcrack density distribution function ρ, is defined as follows:

$$d := \frac{1}{4\pi}\int_S \rho(\mathbf{n})ds, \tag{1}$$

with $\rho(\mathbf{n}) = \rho(-\mathbf{n})$ a scalar and dimensionless measure of the extent of crack-like defects orthogonal to unit vector $\mathbf{n}$, $\mathcal{S} = \left\{\mathbf{n}\in\mathbb{R}^3, \mathbf{n}\cdot\mathbf{n} = 1\right\}$ the unit sphere and ds the infinitesimal surface element on $\mathcal{S}$. Variable d thus corresponds to the density of all microcracks within the representative volume.

The free energy per unit volume, depending on the linearized strain tensor $\mathbf{e}$, is chosen on the form :

$$W(\mathbf{e},d) := W_0(\mathbf{e}) + \frac{1}{4\pi}\int_S w(d,\mathbf{e},\mathbf{n})\ ds \tag{2}$$

where $W_0(\mathbf{e}) := \frac{1}{2}(2\mu_0\mathbf{e}\cdot\mathbf{e} + \lambda_0(\mathrm{tr}\mathbf{e})^2)$ is the free energy of the undamaged material, assumed to be isotropic and linear elastic with Lamé's constants λ_0 and μ_0, $\mathbf{e} := \frac{1}{2}(\nabla\mathbf{u} + \nabla^T\mathbf{u})$ is the linearized strain tensor, with $\mathbf{u}$ the displacement field, and $\mathrm{tr}\mathbf{A} := \mathbf{A}\cdot\mathbf{I}$ represents the trace of tensor $\mathbf{A}$, with $\mathbf{I}$ the identity tensor. The elementary energy function w that characterizes the energy modification induced by each set of parallel microcracks is assumed to be linear with respect to the density, and supposed to account for the different contribution of microcracks whether they are opened or closed, so that:

$$w(d,\mathbf{e},\mathbf{n}) := d\ h(\mathbf{e},\mathbf{n}), \tag{3}$$

with

$$h(\mathbf{e},\mathbf{n}) := \begin{cases} h_{open}(\mathbf{e},\mathbf{n}) & \text{for} \quad g(\mathbf{e},\mathbf{n}) > 0, \\ h_{clos}(\mathbf{e},\mathbf{n}) & \text{for} \quad g(\mathbf{e},\mathbf{n}) \le 0, \end{cases} \tag{4}$$

where function g represents the opening-closure criterion of microcracks. The general expressions of functions h_{open}, h_{clos} and g can be determined considering the representation theories of tensorial functions in terms of $\mathbf{e}$ and $\mathbf{n}^{\otimes 2}$ and the continuity conditions for the nonlinear (multilinear) behavior, since W must be of class C^1. A last requirement is the account of the recovery of properties induced by the closure of microcracks, which is based on micromechanical considerations [42]. Following [19,20], the energy function associated with a given microcrack state is written as

$$h(\mathbf{e},\mathbf{n}) := \alpha\,\mathbf{e}\cdot\mathbf{e} + \beta\,(\operatorname{tr}\mathbf{e})^2 + \chi\,\operatorname{tr}\mathbf{e}\,(\mathbf{e}\cdot\mathbf{n}^{\otimes 2}) + \varphi\,\mathbf{e}^2\cdot\mathbf{n}^{\otimes 2} + \psi\,\left(\operatorname{tr}(\mathbf{e}\,\mathbf{n}^{\otimes 2})\right)^2. \tag{5}$$

In this expression, $h(\cdot)$ denotes either $h_{open}(\cdot)$ or $h_{clos}(\cdot)$, depending on whether the microcracks are open or closed, respectively. Accordingly, the ten coefficients $\{\alpha,\beta,\chi,\varphi,\psi\}$ take the values associated with the considered microcrack state, namely $\{\alpha_{open},\beta_{open},\chi_{open},\varphi_{open},\psi_{open}\}$ for open microcracks and $\{\alpha_{clos},\beta_{clos},\chi_{clos},\varphi_{clos},\psi_{clos}\}$ for closed microcracks. These material parameters are not independent, since they are related through continuity and recovery conditions. Moreover the opening-closure criterion takes the form :

$$g(\mathbf{e},\mathbf{n}) = \delta_1\,\mathbf{e}\cdot\mathbf{n}^{\otimes 2} + \delta_2\operatorname{tr}\mathbf{e}, \tag{6}$$

where δ_1 and δ_2 are two material constants. Denoting $\mathcal{S}^{open}(\mathbf{e}) = \{\mathbf{n}\in\mathcal{S},\ g(\mathbf{n},\mathbf{e})>0\}$ and $\mathcal{S}^{clos}(\mathbf{e}) = \{\mathbf{n}\in\mathcal{S},\ g(\mathbf{n},\mathbf{e})\le 0\}$ respectively the open and closure domains, namely the set of normal vectors respectively to open and to closed microcracks, the thermodynamic potential can be decomposed in this way:

$$\begin{aligned} W(\mathbf{e},d) &= W_0(\mathbf{e}) + \frac{d}{4\pi}\int_{\mathcal{S}^{open}(\mathbf{e})} h_{open}(\mathbf{e},\mathbf{n})ds \\ &\quad + \tfrac{d}{4\pi}\textstyle\int_{\mathcal{S}^{clos}(\mathbf{e})} h_{clos}(\mathbf{e},\mathbf{n})ds \\ &= W_0(\mathbf{e}) + \frac{d}{4\pi}\int_{\mathcal{S}} h_{open}(\mathbf{e},\mathbf{n})ds \\ &\quad - \tfrac{d}{4\pi}\textstyle\int_{\mathcal{S}^{clos}(\mathbf{e})}[h_{open}-h_{clos}](\mathbf{e},\mathbf{n})ds \end{aligned} \tag{7}$$

since $\mathcal{S} = \mathcal{S}^{open}(\mathbf{e}) \cup \mathcal{S}^{clos}(\mathbf{e})$ and $\mathcal{S}^{open}(\mathbf{e}) \cap \mathcal{S}^{clos}(\mathbf{e}) = \emptyset$, whatever $\mathbf{e}$. Accordingly, one obtains the following global form for the free energy:

$$W(\mathbf{e},d) = W_0(\mathbf{e}) + W_{open}(\mathbf{e},d) - \frac{d}{4\pi}\int_{\mathcal{S}^{clos}(\mathbf{e})}[h_{open}-h_{clos}](\mathbf{e},\mathbf{n})ds, \tag{8}$$

where $W_{\mathrm{open}}(\mathbf{e},d)$ denotes the damage contribution to the free energy when all microcracks are open, whereas the last term accounts for the modification induced by crack closure. Since the functions h and g are positively homogeneous with respect to $\mathbf{e}$, of degree two and degree one, respectively, the continuity requirements imposed on the potential W lead to the following conditions [22]:

$$[h_{open}-h_{clos}](\mathbf{e},\mathbf{n}) = \frac{1}{2}\mathbf{e}\cdot(\mathbf{H}\ \mathbf{e}) = \frac{\Delta}{2}\mathbf{e}\cdot(\mathbf{G}\ \mathbf{e}) = \frac{\Delta}{2}g^2(\mathbf{e},\mathbf{n}), \tag{9}$$

where $\mathbf{H} := \frac{\partial^2[h_{open}-h_{clos}]}{\partial\mathbf{e}^2}$ and $\mathbf{G} := \frac{\partial g}{\partial\mathbf{e}}\otimes\frac{\partial g}{\partial\mathbf{e}}$. As $\int_{\mathcal{S}} ds = 4\pi$, relevant calculations lead to such simplified form of Eq. (8):

$$W(\mathbf{e},d) = W_0(\mathbf{e}) + d\left(\alpha\mathbf{e}\cdot\mathbf{e} + \beta(\operatorname{tr}\mathbf{e})^2 - \frac{\Delta}{8\pi}\int_{\mathcal{S}^{clos}(\mathbf{e})} g^2(\mathbf{e},\mathbf{n})ds\right) \tag{10}$$

where α, β, and Δ are independent constitutive parameters. Within the free energy, the terms in α and β thus define the damage contribution to energy when microcracks are all open, while the integral part is related to its variation due to the possible closure of some defects, according to the loading. The influence of this latter term on the effective mechanical properties of microcracked materials has been investigated in [19,20] (see also [22] for the stress-based version of the model). In particular, considering an initially isotropic damage state, characterized by an equal microcracks density in all direction of space, the partial closure of microcracks induces an anisotropic mechanical response, as discussed in [21].

The constitutive parameters α and β can be identified on the basis of micromechanical arguments. Consider a representative volume element of a homogeneous, isotropic, linear elastic matrix weakened by an array of randomly distributed, flat penny-shaped microcracks. Assuming a dilute concentration of non-interacting and frictionless microcracks, the free energy of the microcracked medium, depending on the microcracks state (open or closed), can be derived through several approaches. These include: (i) the application of the Legendre-Fenchel's transform to the free enthalpy [43]; (ii) a strain-based formulation relying on crack displacement jumps [44]; and (iii) Eshelby's method applied to thin ellipsoidal defects [45]. These approaches enable the determination of α and β from the configuration of all open cracks the expression of α and β, either in terms of the Lamé's coefficients λ_0 and μ_0:

$$\begin{aligned} \alpha &= -\frac{16\mu_0(\lambda_0+2\mu_0)(9\lambda_0+10\mu_0)}{45(\lambda_0+\mu_0)(3\lambda_0+4\mu_0)}, \\ \beta &= -\frac{2\lambda_0(\lambda_0+2\mu_0)(45\lambda_0^2+120\lambda_0\mu_0+76\mu_0^2)}{45\mu_0(\lambda_0+\mu_0)(3\lambda_0+4\mu_0)}. \end{aligned} \tag{11}$$

or, equivalently, from the undamaged Young's modulus E_0 and shear modulus μ_0:

$$\begin{aligned} \alpha &= \frac{16(E_0-12\mu_0)(E_0-4\mu_0)}{45\ (E_0-6\mu_0)}, \\ \beta &= -\frac{2(E_0-4\mu_0)(E_0-2\mu_0)(E_0^2-36E_0\mu_0+144\mu_0^2)}{45(E_0-6\mu_0)\ (E_0-3\mu_0)^2}. \end{aligned} \tag{12}$$

The above relations imply that α and β are both negative coefficients.

2.2. Special case under study

In the present paper, a special case of the opening-closure criterion (6) will be taken into account. Considering $\delta_1 = 0$, one has:

$$g(\mathbf{e},\mathbf{n}) = g(\mathbf{e}) = \delta_2\operatorname{tr}\mathbf{e}.$$

Since the criterion is independent of the normal $\mathbf{n}$ to cracks, microcracks can only be either all opened or all closed, and the material remains isotropic. In this case, the thermodynamic potential reduces to:

$$W(\mathbf{e},d) = W_0(\mathbf{e}) + d\left[\alpha\mathbf{e}\cdot\mathbf{e} + \left(\beta - \frac{\Omega}{8\pi}\int_{\mathcal{S}^{clos}(\mathbf{e})} ds\right)\ (\mathrm{tr}\mathbf{e})^2\right], \tag{13}$$

with $\Omega := \Delta\delta_2^2 = \dfrac{2(\alpha+3\beta)}{3}$. Hence, one has:

- for all opened cracks, i.e., $g(\mathbf{e}) > 0$ and $\mathcal{S}^{clos}(\mathbf{e}) = \varnothing$:

$$W(\mathbf{e},d) = W_0(\mathbf{e}) + d\left[\alpha\mathbf{e}\cdot\mathbf{e} + \beta(\mathrm{tr}\mathbf{e})^2\right], \tag{14}$$

- for all closed cracks, i.e., $g(\mathbf{e}) \le 0$ and $\mathcal{S}^{clos}(\mathbf{e}) = \mathcal{S}$:

$$W(\mathbf{e},d) = W_0(\mathbf{e}) + d\left[\alpha'\mathbf{e}\cdot\mathbf{e} + \beta'\ (\mathrm{tr}\mathbf{e})^2\right], \tag{15}$$

with $\alpha' = \alpha$ and $\beta' = \beta - \dfrac{\Omega}{2} = -\dfrac{\alpha}{3}$.

From the thermodynamic potential, it is possible to derive the constitutive laws in terms of the Cauchy's stress tensor σ and the scalar thermodynamic force related to damage F_d. As continuity conditions on coefficients $\{\alpha_{open},\beta_{open},\chi_{open},\varphi_{open},\psi_{open}\}$ and $\{\alpha_{clos},\beta_{clos},\chi_{clos},\varphi_{clos},\psi_{clos}\}$ have been met to ensure that W (and thus h) is of class C^1, they are defined by:

$$\begin{cases} \sigma = \dfrac{\partial W}{\partial\mathbf{e}} = \dfrac{\partial W_0}{\partial\mathbf{e}} + \dfrac{d}{4\pi}\displaystyle\int_{\mathcal{S}}\dfrac{\partial h(\mathbf{e})}{\partial\mathbf{e}}ds, \\ F_d = -\dfrac{\partial W}{\partial d} = -\dfrac{1}{4\pi}\displaystyle\int_{\mathcal{S}} h(\mathbf{e})ds \end{cases} \tag{16}$$

Introducing the same decomposition on $\mathcal{S}^{open}(\mathbf{e})$ and $\mathcal{S}^{clos}(\mathbf{e})$ used to simplify the form of the free energy in Eq. (7), we thus get:

$$\begin{cases} \sigma = \lambda_0(\mathrm{tr}\mathbf{e})\mathbf{I} + 2\mu_0\mathbf{e} + 2d\left[\alpha\mathbf{e} + \left(\beta - \dfrac{\Omega}{8\pi}\displaystyle\int_{\mathcal{S}^{clos}(\mathbf{e})} ds\right)(\mathrm{tr}\mathbf{e})\mathbf{I}\right], \\ F_d = -\left[\alpha\mathbf{e}\cdot\mathbf{e} + \left(\beta - \dfrac{\Omega}{8\pi}\displaystyle\int_{\mathcal{S}^{clos}(\mathbf{e})} ds\right)\ (\mathrm{tr}\mathbf{e})^2\right], \end{cases} \tag{17}$$

that makes appear again the damage contribution when all microcracks are open and the modification induced by closed microcracks. More specifically, the above constitutive relations can be rewritten as follows:

$$\boldsymbol{\sigma} = \begin{cases} \lambda(d)(\mathrm{tr}\mathbf{e})\mathbf{I} + 2\mu(d)\mathbf{e} & \text{for} \quad g(\mathbf{e}) > 0, \\ \lambda'(d)(\mathrm{tr}\mathbf{e})\mathbf{I} + 2\mu(d)\mathbf{e} & \text{for} \quad g(\mathbf{e}) \le 0, \end{cases} \tag{18}$$

$$F_d = \begin{cases} -\left(\alpha\mathbf{e}\cdot\mathbf{e} + \beta(\mathrm{tr}\mathbf{e})^2\right) & \text{for} \quad g(\mathbf{e}) > 0, \\ -\left(\alpha\mathbf{e}\cdot\mathbf{e} - \frac{\alpha}{3}(\mathrm{tr}\mathbf{e})^2\right) & \text{for} \quad g(\mathbf{e}) \le 0, \end{cases} \tag{19}$$

where $\lambda(d) := \lambda_0 + 2\beta d$, $\lambda'(d) := \lambda_0 - \frac{2}{3}\alpha d$ and $\mu(d) := \mu_0 + \alpha d$.

2.3. Damage evolution law

The evolution of damage is formulated within the classical framework of thermodynamics with internal variables. A single dissipative mechanism is assumed, namely the initiation and growth of microcracks, which are considered non-interacting at the microscale. The damage process is modeled as progressive and rate independent, implying that its evolution depends exclusively on the loading history. Consistently with this assumption, dissipation is governed by a scalar dissipation potential of the form:

$$\mathcal{D}(\dot{d}, d) = \mathcal{R}(d)\,\dot{d}, \tag{20}$$

where $\dot{d}$ denotes the damage evolution rate. Following the approach by J.J. Marigo [46], the resistance function $\mathcal{R}(d)$ is assumed to depend linearly on the damage variable,

$$\mathcal{R}(d) = k_0(1 + \eta d), \tag{21}$$

with $k_0 > 0$ representing the initial damage resistance and $\eta > 0$ controlling its evolution as damage progresses. These two coefficients should be identified through experimental tests on the material [19]: the parameter k_0 may be determined from the damage initiation point while the coefficient η makes it possible to account for positive or negative work hardening in the non-linear stress–strain response, with special cases of pure brittle behavior after damage initiation (if $\eta = 0$) or non-evolving damage (if $\eta \to \infty$). Considering the dissipation potential (20) ensures positive dissipation and provides a physically motivated description of the increasing resistance to further microcrack growth. Combining this damage functions with the normality rule, the damage evolution law reads:

$$\begin{cases} \dot{d} = \dot{\Lambda}\frac{\partial f}{\partial F^d}(F^d, d) = \dot{\Lambda} & \\ \dot{\Lambda} = 0 & \text{for} \quad f(F_d, d) < 0, \\ \dot{\Lambda} = 0 & \text{for} \quad f(F_d, d) = 0, \quad \dot{f}(F_d, d) < 0, \\ \dot{\Lambda} = \frac{\langle \dot{F}_d \rangle_+}{k_0\eta} > 0 & \text{for} \ f(F_d, d) = 0, \quad \dot{f}(F_d, d) = 0, \end{cases} \tag{22}$$

where $f(F_d, d) := F_d - \mathcal{R}(d)$ represents the yield function, $\langle f \rangle_+ := \mathrm{Max}\{0, f\}$ is the positive part of f, equivalent to the Macaulay's brackets, and $\dot{\Lambda}$ denotes the damage multiplier, determined by the consistency condition [19,47].

3. Statement of the problem

In the sequel, an orthonormal Cartesian reference frame $(O; \mathbf{i}_1, \mathbf{i}_2, \mathbf{i}_3)$ is introduced, and the coordinates (x_1, x_2, x_3) are used to identify a generic material point. Let us consider a composite assembly made of three media, two adherents and a thin adhesive layer, occupying a smooth bounded domain $\Omega^\varepsilon \subset \mathbb{R}^3$, as depicted in Fig. 1(a).

The domain $\Omega^\varepsilon := \Omega^\varepsilon_+ \cup B^\varepsilon \cup \Omega^\varepsilon_-$ depends on the parameter ε, as follows: (i) the adhesive layer occupies the domain $B^\varepsilon := \left\{(x_1, x_2, x_3) \in \Omega^\varepsilon : |x_3| < \frac{h^\varepsilon}{2}\right\}$, where h^ε denotes its thickness; (ii) its plane mid-surface is given by $S := \left\{(x_1, x_2, x_3) \in \Omega^\varepsilon : x_3 = 0\right\}$, which represents the interface in the limit problem; (iii) the adherents occupy the subdomains $\Omega^\varepsilon_\pm := \left\{(x_1, x_2, x_3) \in \Omega^\varepsilon : \pm x_3 > \frac{h^\varepsilon}{2}\right\}$; (iv) the interfaces between the adhesive and the adherents are denoted by $S^\varepsilon_\pm := \left\{(x_1, x_2, x_3) \in \Omega^\varepsilon : x_3 = \pm\frac{h^\varepsilon}{2}\right\}$.

The asymptotic expansion developed below relies on the classical thin-layer hypothesis, namely that the adhesive thickness is much smaller than the characteristic dimensions of the bonded structure. Accordingly, the small parameter ε is introduced through the relation $h^\varepsilon = \varepsilon h$, with $\varepsilon \ll 1$. Moreover, the interfaces are assumed to be geometrically regular and homogeneous at the macroscopic scale. In particular, effects related to surface roughness, local thickness variations, or spatially non-uniform adhesive properties along the interface are not included in the present formulation. The loading process is assumed to be quasi-static and body forces inside the adhesive layer B^ε are neglected. The structure is subjected to body forces $\mathbf{f}^\varepsilon$, acting in $\Omega^\varepsilon_\pm$, and to surface tractions $\mathbf{g}^\varepsilon$, applied on a portion of the boundary $\Gamma^\varepsilon_g \subset \partial\Omega^\varepsilon$ with strictly positive measure. The composite is fully clamped on another portion of the boundary $\Gamma^\varepsilon_0 \subset \partial\Omega^\varepsilon$. The boundary sets Γ^ε_g and Γ^ε_0 are assumed to be located sufficiently far from the interphase. Appropriate regularity assumptions on the external loads are introduced to guarantee the well-posedness of the equilibrium problem.

As customary, the governing equations of the equilibrium problem, paired with the constitutive laws (24), can be written :

$$\begin{cases} \mathrm{div}^\varepsilon\boldsymbol{\sigma}^\varepsilon + \mathbf{f}^\varepsilon = \mathbf{0} & \text{in } \Omega^\varepsilon, \\ \boldsymbol{\sigma}^\varepsilon\mathbf{n}^\varepsilon = \mathbf{g}^\varepsilon & \text{on } \Gamma^\varepsilon_g, \\ [\![\boldsymbol{\sigma}^\varepsilon\mathbf{i}_3]\!] = \mathbf{0} & \text{on } S^\varepsilon_\pm, \\ [\![\mathbf{u}^\varepsilon]\!] = \mathbf{0} & \text{on } S^\varepsilon_\pm, \\ \mathbf{u}^\varepsilon = \mathbf{0} & \text{on } \Gamma^\varepsilon_0, \end{cases} \tag{23}$$

where div^ε denotes the divergence operator, $[\![f]\!]$ is the jump function at the interfaces $S^\varepsilon_\pm$, i.e $[\![f]\!] := \bar{f}(\pm h^\varepsilon/2) - \hat{f}(\pm h^\varepsilon/2)$. In the sequel, if necessary, the notation $\bar{f}$, $\hat{f}$ stands for the restriction of function f in the adherents and in the adhesive, respectively.

The two adherents are assumed to be linearly elastic materials and non-damaging, with constitutive relations specified below:

$$\bar{\boldsymbol{\sigma}}^\varepsilon = \bar{\mathbf{C}}^\varepsilon\mathbf{e}^\varepsilon, \tag{24}$$

where $\bar{\mathbf{C}}^\varepsilon = (\bar{C}^\varepsilon_{ijkl})$ represents the fourth-order elasticity tensor, which satisfies the classical major and minor symmetries properties. The material of the adhesive layer is assumed to be linear elastic, initially isotropic and damaging, and its constitutive law is expressed in Eqs. (18) and (19). Finally, the damage evolution equations are described in (22).

4. Asymptotic expansions method

Given the small thickness of the adhesive layer, namely $h^\varepsilon = \varepsilon h$, we seek the solution of the equilibrium problem by means of an asymptotic expansion with respect to the small parameter ε. In order to apply the asymptotic expansions method, the ε-dependent domain Ω^ε is mapped onto a fixed reference domain Ω through a classical change of variables [48], illustrated in Fig. 1.

- In the adhesive layer, the following rescaling of the transverse coordinate is introduced:

  $$(x_1, x_2, x_3) \in B^\varepsilon \longmapsto (z_1, z_2, z_3) = (x_1, x_2, \tfrac{x_3}{\varepsilon}) \in B, \tag{25}$$

  where $B := \left\{(x_1, x_2, x_3) \in \Omega : |x_3| < \frac{h}{2}\right\}$. Moreover, for any scalar- or vector-valued field v defined on B^ε, we define the rescaled field $\hat{v}(z_1, z_2, z_3) = v(x_1, x_2, x_3)$.

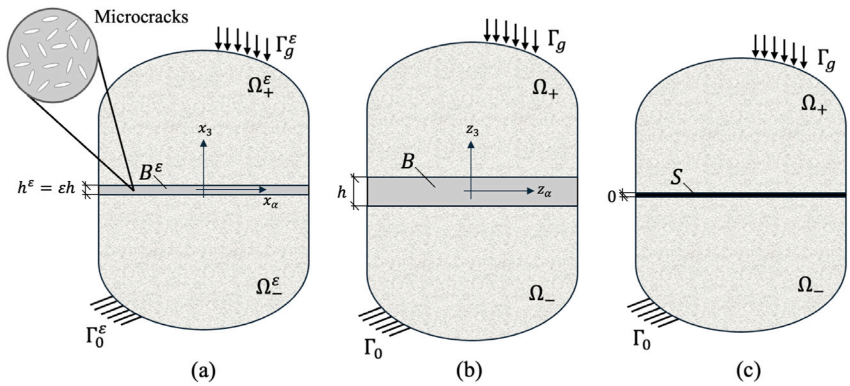

Fig. 1. Geometry of the bonded assembly composed of two adherent bodies and an adhesive thin layer: reference configuration (a), rescaled configuration (b) and limit configuration (c).

- In the adherents, the following change of variables is adopted:

$$(x_1,x_2,x_3)\in\Omega_\pm^\varepsilon \longmapsto (z_1,z_2,z_3)=(x_1,x_2,x_3\pm\tfrac{h}{2}\mp\varepsilon\tfrac{h}{2})\in\Omega_\pm, \quad (26)$$

where $\Omega_\pm := \left\{(x_1,x_2,x_3)\in\Omega:\ \pm x_3>\frac{h}{2}\right\}$. For any scalar- or vector-valued field v defined in $\Omega_\pm^\varepsilon$, we set $\bar v(z_1,z_2,z_3)=v(x_1,x_2,x_3)$.

The volume and surface forces are assumed to be independent of ε, so that $\mathbf{f}^\varepsilon(x_1,x_2,x_3)=\mathbf{f}(z_1,z_2,z_3)$ and $\mathbf{g}^\varepsilon(x_1,x_2,x_3)=\mathbf{g}(z_1,z_2,z_3)$. According to the above change of variables, one has

$$\frac{\partial}{\partial z_\alpha}=\frac{\partial}{\partial x_\alpha},\qquad \frac{\partial}{\partial z_3}=\varepsilon\frac{\partial}{\partial x_3}\quad \text{in } B^\varepsilon.$$

Finally, we assume that the solution of the equilibrium problem admits the following asymptotic expansions:

$$\begin{cases}\hat{\boldsymbol\sigma}^\varepsilon=\hat{\boldsymbol\sigma}^0+\varepsilon\,\hat{\boldsymbol\sigma}^1+o(\varepsilon),\\ \hat{\mathbf{u}}^\varepsilon=\hat{\mathbf{u}}^0+\varepsilon\,\hat{\mathbf{u}}^1+o(\varepsilon),\\ \bar{\boldsymbol\sigma}^\varepsilon=\bar{\boldsymbol\sigma}^0+\varepsilon\,\bar{\boldsymbol\sigma}^1+o(\varepsilon),\\ \bar{\mathbf{u}}^\varepsilon=\bar{\mathbf{u}}^0+\varepsilon\,\bar{\mathbf{u}}^1+o(\varepsilon),\end{cases} \quad (27)$$

where the first two equations are written in the adhesive, and the last two are written in the adherents. Applying the change of variables to the governing Eqs. (23) and substituting the expansions (27) into the rescaled problem yields the leading-order terms and the associated limit problem.

4.1. The strain field

In the rescaled configuration of the adhesive layer, the displacement gradient reads

$$\nabla\hat{\mathbf{u}}^\varepsilon=\frac{1}{\varepsilon}\begin{pmatrix}0&0&\hat u^0_{1,3}\\0&0&\hat u^0_{2,3}\\0&0&\hat u^0_{3,3}\end{pmatrix}+\begin{pmatrix}\hat u^0_{1,1}&\hat u^0_{1,2}&\hat u^1_{1,3}\\ \hat u^0_{2,1}&\hat u^0_{2,2}&\hat u^1_{2,3}\\ \hat u^0_{3,1}&\hat u^0_{3,2}&\hat u^1_{3,3}\end{pmatrix}+o(\varepsilon). \quad (28)$$

where $(\cdot)_{,i}$ denotes the partial derivatives with respect to z_i. Accordingly, the strain tensor admits the expansion

$$\hat{\mathbf{e}}^\varepsilon=\frac{1}{\varepsilon}\hat{\mathbf{e}}^{-1}+\hat{\mathbf{e}}^0+o(\varepsilon), \quad (29)$$

where $\hat{\mathbf{e}}^{-1}:=\hat{\mathbf{u}}^0_{,3}\odot\mathbf{i}_3$, and $\hat{\mathbf{e}}^0:=\hat{\mathbf{u}}^0_{,\alpha}\odot\mathbf{i}_\alpha+\hat{\mathbf{u}}^1_{,3}\odot\mathbf{i}_3$.

Within the rescaled adherents, the displacement gradient takes the form

$$\nabla\bar{\mathbf{u}}^\varepsilon=\begin{pmatrix}\bar u^0_{1,1}&\bar u^0_{1,2}&\bar u^0_{1,3}\\ \bar u^0_{2,1}&\bar u^0_{2,2}&\bar u^0_{2,3}\\ \bar u^0_{3,1}&\bar u^0_{3,2}&\bar u^0_{3,3}\end{pmatrix}+o(\varepsilon), \quad (30)$$

leading to the strain expansion

$$\bar{\mathbf{e}}^\varepsilon=\bar{\mathbf{e}}^0+\varepsilon\bar{\mathbf{e}}^1+o(\varepsilon^2), \quad (31)$$

with $\bar{\mathbf{e}}^p:=\bar{\mathbf{u}}^p_{,i}\odot\mathbf{i}_i$, $p\geq 0$.

4.2. The equilibrium equations

The governing Eqs. (23) can be rewritten in the rescaled configuration. Considering the equilibrium equations in the adhesive layer and exploiting the asymptotic expansion of the stress field (27), one obtains

$$0=\frac{1}{\varepsilon}\hat\sigma^\varepsilon_{i3,3}+\hat\sigma^\varepsilon_{i\alpha,\alpha}=\frac{1}{\varepsilon}\hat\sigma^0_{i3,3}+\hat\sigma^0_{i\alpha,\alpha}+\hat\sigma^1_{i3,3}+o(\varepsilon). \quad (32)$$

By sorting the terms with the identical power of ε, we get

$$\hat\sigma^0_{i3,3}=0, \quad (33)$$

which implies that $\hat\sigma^0_{i3}$ is independent of the thickness coordinate z_3. The continuity of the stress vector across the adhesive–adherent interfaces then leads to

$$[\![\hat\sigma^0_{i3}]\!]=0, \quad (34)$$

meaning that the jump of the stress vector vanishes at $z_3=\pm h/2$.

The rescaled equilibrium equations in the adherents read

$$\mathrm{div}\bar{\boldsymbol\sigma}^0+\mathbf{f}=\mathbf{0}\quad \text{in } \Omega_\pm,\qquad \bar{\boldsymbol\sigma}^0\mathbf{n}=\mathbf{g}\quad \text{on } \Gamma_g. \quad (35)$$

The displacement and the stress vector are continuous across the interfaces $S^\varepsilon_\pm$ and $S_\pm$, in the reference and rescaled configurations, respectively. From displacement continuity, one has

$$\mathbf{u}^\varepsilon(\tilde{\mathbf{x}},\pm\varepsilon h/2)=\bar{\mathbf{u}}^\varepsilon(\tilde{\mathbf{z}},\pm h/2)=\hat{\mathbf{u}}^\varepsilon(\tilde{\mathbf{z}},\pm h/2),\quad \tilde{\mathbf{x}}=(x_\alpha),\ \tilde{\mathbf{z}}=(z_\alpha)\in S. \quad (36)$$

Expanding the displacement in a Taylor's series with respect to x_3 and using (27), it follows that

$$\mathbf{u}^\varepsilon(\tilde{\mathbf{x}},\pm\varepsilon h/2)=\mathbf{u}^\varepsilon(\tilde{\mathbf{x}},0^\pm)+o(\varepsilon)=\mathbf{u}^0(\tilde{\mathbf{x}},0^\pm)+o(\varepsilon). \quad (37)$$

Thanks to the continuity conditions, we have:

$$\mathbf{u}^0(\tilde{\mathbf{x}},0^\pm)+o(\varepsilon)=\bar{\mathbf{u}}^0(\tilde{\mathbf{z}},\pm h/2)+o(\varepsilon)=\hat{\mathbf{u}}^0(\tilde{\mathbf{z}},\pm h/2)+o(\varepsilon), \quad (38)$$

and therefore

$$\mathbf{u}^0(\tilde{\mathbf{x}},0^\pm)=\bar{\mathbf{u}}^0(\tilde{\mathbf{z}},\pm h/2)=\hat{\mathbf{u}}^0(\tilde{\mathbf{z}},\pm h/2). \quad (39)$$

Analogous arguments can be applied to the stress field, leading to

$$[\sigma^0_{i3}]=0, \quad (40)$$

where $[f]:=f(\tilde{\mathbf{x}},0^+)-f(\tilde{\mathbf{x}},0^-)$ denotes the jump of a quantity across the limit interface S as $\varepsilon\to 0$, see Fig. 1(c). The above results imply that the stress vector evaluated at the level of the interface is continuous and, thus, $[\boldsymbol\sigma^0\mathbf{i}_3]=\mathbf{0}$.

4.3. The constitutive laws and the damage evolution equations

Since the material of the adhesive is assumed to be soft, i.e., mechanically compliant, the undamaged Lamé's constants are assumed to depend linearly on ε, so that $\hat{\lambda}_0^\varepsilon = \varepsilon\hat{\lambda}_0$ and $\hat{\mu}_0^\varepsilon = \varepsilon\hat{\mu}_0$. Same scaling assumptions are used for the material coefficients related to damage, namely $\hat{\alpha}^\varepsilon = \varepsilon\hat{\alpha}$ and $\hat{\beta}^\varepsilon = \varepsilon\hat{\beta}_0$. Consequently, the scaling of the damaging Lamé's constants is $\hat{\lambda}^\varepsilon(d) := \varepsilon(\hat{\lambda}_0 + 2\hat{\beta}d) = \varepsilon\hat{\lambda}(d)$, $\hat{\lambda}'^\varepsilon(d) := \varepsilon(\hat{\lambda}_0 - \frac{2}{3}\hat{\alpha}d) = \varepsilon\hat{\lambda}'(d)$, and $\mu^\varepsilon(d) := \varepsilon(\hat{\mu}_0 + \hat{\alpha}d) = \varepsilon\hat{\mu}(d)$. Moreover, the opening-closure criterion is assumed to be such that: $\hat{g}^\varepsilon = \varepsilon\hat{g}$. Let us recall that $\hat{\alpha}$ and $\hat{\beta}$ are assumed to satisfy the same micromechanical relations as the corresponding bulk coefficients α and β, defined in Eqs. (11)–(12). Under the usual elastic admissibility conditions for the undamaged adhesive, these relations imply $\hat{\alpha} < 0$, and $\hat{\beta} < 0$, and, thus, $-(\hat{\alpha} + \hat{\beta}) > 0$.

Considering the adhesive constitutive law (18) at order 0, one has

$$\hat{\sigma}_{i3}^0 = \begin{cases} \hat{\mu}(d)\hat{u}_{i,3}^0 + (\hat{\lambda}(d) + \hat{\mu}(d))\hat{u}_{3,3}^0\delta_{i3} & \text{for} \quad \hat{u}_{3,3}^0 > 0, \\ \hat{\mu}(d)\hat{u}_{i,3}^0 + (\hat{\lambda}'(d) + \hat{\mu}(d))\hat{u}_{3,3}^0\delta_{i3} & \text{for} \quad \hat{u}_{3,3}^0 \leq 0. \end{cases} \tag{41}$$

The independence of $\hat{\sigma}_{i3}^0$ with respect to the thickness coordinate leads to $\hat{u}_{i,3}^0$ to be also does independent of z_3, and thus, $\hat{u}_i^0$ is linear in terms of z_3. The continuity conditions of the displacements at the interface entails that $\hat{\mathbf{u}}_{,3}^0 = \frac{[\mathbf{u}^0]}{h}$. By substituting the results in (41), we obtain the following explicit expression of the stress vector at the level of the interface:

$$\hat{\boldsymbol{\sigma}}^0\mathbf{i}_3 = \begin{cases} \frac{1}{h}(\hat{\mu}(d)[\mathbf{u}^0] + (\hat{\lambda}(d) + \hat{\mu}(d))[u_3^0]\mathbf{i}_3) & \text{for} \quad [u_3^0] > 0, \\ \frac{1}{h}(\hat{\mu}(d)[\mathbf{u}^0] + (\hat{\lambda}'(d) + \hat{\mu}(d))[u_3^0]\mathbf{i}_3) & \text{for} \quad [u_3^0] \leq 0. \end{cases} \tag{42}$$

Notably, the normal stiffness of the interfacial law, $\hat{\lambda}(d) + 2\hat{\mu}(d)$, depends on the sign of $[u_3^0]$. In particular, when $[u_3^0] > 0$, e.g., in the presence of debonding, the normal stiffness vanishes at the critical damage level

$$d_{crit}^+ := -\frac{\hat{\lambda}_0 + 2\hat{\mu}_0}{2(\hat{\alpha} + \hat{\beta})}. \tag{43}$$

Conversely, when $[u_3^0] \leq 0$, e.g., in the presence of contact, the normal stiffness vanishes at

$$d_{crit}^- := -\frac{3(\hat{\lambda}_0 + 2\hat{\mu}_0)}{4\hat{\alpha}}. \tag{44}$$

Damage levels above and below these critical values are not admissible, as the normal stiffness would become negative. Thus, the levels $d_{crit}^\pm$ identify full damage at debonding and at closure. Interestingly, if $\hat{\lambda}_0 > -2\hat{\mu}_0/3$, then $d_{crit}^+ < d_{crit}^-$, implying that the model allows full damage to occur later in contact than under debonding. Such behavior is fully consistent with the damage evolution observed at the bulk material scale [3,42]. As observed for rocks and concrete, damage initiation occurs at higher load levels and evolves more slowly under axial compression than under axial tension. Under tensile loading, defects are open regardless of their orientation. In contrast, under compressive loading, some cracks, particularly those whose normal is nearly aligned with the loading axis, tend to close. As a result, compression produces a delayed and progressive damage evolution, since closed cracks contribute less to damage mechanisms.

The tangential stiffness of the interfacial law vanishes at the same critical damage level for both debonding and contact:

$$d_{crit}^t := -\frac{\mu_0}{\hat{\alpha}}. \tag{45}$$

This observation is again consistent with the assumptions underlying the adopted damage model. In particular, this refers to the recovery condition associated with microcrack closure. The corresponding restoration of elastic properties derives from the micromechanical analysis of frictionless microcracks, following the same identification procedure used for the parameters α and β (see Section 2.1). Within this framework, a set of closed microcracks does not to contribute to the degradation of the elongation modulus along their normal direction, nor to the degradation of the volumetric modulus in any spatial direction. As shown in [42], closed defects can only undergo frictionless sliding; consequently, the shear modulus is unaffected by microcrack closure and no stiffness recovery occurs in shear. Accordingly, the tangential stiffness remains independent of the crack state, and thus, of debonding and contact conditions.

Let us now consider the thermodynamic damage force $\hat{F}_d^\varepsilon$, expressed in (19). By applying the change of coordinates, the scaling of the material constants and assuming an asymptotic development $\hat{F}_d^\varepsilon = \frac{1}{\varepsilon}\hat{F}_d^{(-1)} + \hat{F}_d^0 + o(\varepsilon)$, the thermodynamic force at the lowest order of ε, takes the following expression in terms of the jump of the displacements:

$$\hat{F}_d^{(-1)} = \begin{cases} -\frac{1}{h^2}\left(\frac{\hat{\alpha}}{2}([u_1^0]^2 + [u_2^0]^2) + (\hat{\alpha} + \hat{\beta})[u_3^0]^2\right) & \text{for} \quad [u_3^0] > 0, \\ -\frac{1}{h^2}\left(\frac{\hat{\alpha}}{2}([u_1^0]^2 + [u_2^0]^2) + \frac{2\hat{\alpha}}{3}[u_3^0]^2\right) & \text{for} \quad [u_3^0] \leq 0. \end{cases} \tag{46}$$

The constitutive coefficient of the adherents are assumed to be independent of ε, so that $\bar{\mathbf{C}}^\varepsilon = \bar{\mathbf{C}}$. Substituting the expansions of the rescaled displacement and stress into the constitutive equations of the adherents, we obtain the following relations:

$\bar{\boldsymbol{\sigma}}^0 = \bar{\mathbf{C}}\bar{\mathbf{e}}^0$.

Finally, the damage evolution Eqs. (22) can be rewritten at the lowest order, taking into account the results obtained in the previous sections. Indeed, considering the following scaling $\hat{k}_0^\varepsilon = \frac{1}{\varepsilon}\hat{k}_0$ and $\hat{\eta}^\varepsilon = \hat{\eta}$, the resistance function takes the form: $\hat{\mathcal{R}}_d^\varepsilon = \frac{1}{\varepsilon}\hat{k}_0(1 + \hat{\eta}d)$. Thus, we obtain:

$$\begin{cases} \dot{d} = 0 & \text{for} \;\; \tilde{f}(\hat{F}_d^{(-1)}, d) = 0, \quad \dot{\tilde{f}}(\hat{F}_d^{(-1)}, d) < 0, \\ \dot{d} = 0 & \text{for} \;\; \tilde{f}(\hat{F}_d^{(-1)}, d) < 0, \\ \dot{d} = \frac{\left\langle \dot{\hat{F}}_d^{(-1)} \right\rangle_+}{\hat{k}_0\hat{\eta}} > 0 & \text{for} \;\; \tilde{f}(\hat{F}_d^{(-1)}, d) = 0, \quad \dot{\tilde{f}}(\hat{F}_d^{(-1)}, d) = 0, \end{cases} \tag{47}$$

where $\tilde{f}(\hat{F}_d^{(-1)}, d) := \hat{F}_d^{(-1)} - \hat{k}_0(1 + \hat{\eta}d)$.

Remark 1. The above scaling corresponds to the soft-interface model considered in the present work. In particular, the linear dependence on ε of the undamaged Lamé coefficients, $\hat{\lambda}_0^\varepsilon$ and $\hat{\mu}_0^\varepsilon$, which is typical of soft-interface asymptotic regimes, naturally entails the same scaling for the damage-related coefficients $\hat{\alpha}^\varepsilon$ and $\hat{\beta}^\varepsilon$, since these parameters enter the adhesive constitutive law through the damaged elastic moduli. This choice yields finite interfacial tractions and finite displacement jumps at the leading order of the expansion. Moreover, since the thermodynamic force associated with damage is quadratic in the strain, the scaling $\hat{k}_0^\varepsilon = \frac{\hat{k}_0}{\varepsilon}$ is required in order to obtain a non-trivial damage criterion in the limit problem. Other scalings are possible and would lead to different asymptotic regimes: stiffer layers would tend to perfect-interface conditions at leading order, whereas softer layers would lead to vanishing tractions or degenerate interface laws, unless different load or displacement scalings were introduced.

5. Application of the interface damage model to a butt joint

In this Section, the interface damage model derived above is applied to simulate the damaging behavior of the adhesive in a symmetric butt joint under normal loading. Our aim is to investigate the macroscopic force–displacement response and the damage evolution under hard and soft loading devices.

The joint consists of two identical adherent blocks, $\Omega_\pm$, with the same L and height $H_\pm$, in contact via the damaging interface model described by Eqs. (34), (42), (46) and (47). The composite structure undergoes axial loading in the direction of the x_3-axis, perpendicular to the adhesive's plane.

The two adherents are composed of the same isotropic and linear elastic material, with engineering constants E, ν. The adhesive's thickness is denoted h, so that the total height of the composite is H_{tot} =

$H_+ + H_- + h$. Under a soft loading device, body forces are neglected and uniform normal surface forces of intensity q_3 are applied to the upper and lower bases of the composite. Under a hard loading device, a relative normal displacement Δ along the x_3-axis is applied to the upper and lower bases of the composite, and q_3 are the corresponding surface reaction forces.

In the two adherents, the stress tensor is assumed to take the simple form

$$\bar{\sigma} = q_3\,(\mathbf{i}_3 \otimes \mathbf{i}_3), \tag{48}$$

where $\mathbf{i}_3$ is the unit vector of the x_3-axis. With this choice, the transmission conditions (34) and the equilibrium Eqs. (35) are identically satisfied.

Let $\bar{\mathbf{u}}_\pm$ be taken to denote the displacement field in $\Omega_\pm$. The constitutive equations in $\Omega_\pm$ and the compatibility conditions within the adhesive require that

$$\bar{\mathbf{u}}_\pm(\mathbf{x}) = \left(-\frac{\nu\, q_3}{E}x_\alpha \pm \frac{[u_\alpha]}{2}\right)\mathbf{i}_\alpha + \left(\frac{q_3}{E}x_3 \pm \frac{[u_3]}{2}\right)\mathbf{i}_3, \tag{49}$$

where $\mathbf{x} \in \Omega_\pm$, and $[u_i]$, $i = 1,2,3$, are the displacement jumps across the damaging interface S, modeling the damaging thin adhesive layer.

The macroscopic response of the composite is characterized by its force–displacement response, $P - \Delta$, where

$$\Delta := (\bar{\mathbf{u}}_+|_{x_3=H_+ + h/2} - \bar{\mathbf{u}}_-|_{x_3=-H_- - h/2}) \cdot \mathbf{i}_3 \tag{50}$$

is the macroscopic normal displacement, and P is the macroscopic normal force

$$P(t) = q_3 A, \tag{51}$$

where A is the bonding area. In view of Eqs. (49) and (50), the jump $[u_3]$ is linked to the force P and to the macroscopic normal displacement Δ as follows:

$$[u_3] = \Delta - \frac{P}{EA}H_{tot}. \tag{52}$$

By substituting the expression of the stress in the adherents (48) into (42), and using (34) and (52), we find that the in-plane jumps across the interface vanish, $[u_\alpha] = 0, \alpha = 1,2$, and that the following force–displacement relation holds:

$$P = \frac{\chi(d)}{(1+\chi(d))}\frac{EA}{H_{tot}}\Delta, \tag{53}$$

where

$$\chi(d) := c_1 - c_2 d, \quad c_1 := \frac{H_{tot}}{h}\frac{\hat{\lambda}_0 + 2\hat{\mu}_0}{E}, \quad c_2 := \frac{H_{tot}}{h}\frac{2\hat{\gamma}}{E}. \tag{54}$$

in which $c_1 > 0$. The material parameter $\hat{\gamma}$ has different values for contact and debonding. It is defined as follows:

$$\hat{\gamma} := \begin{cases} -(\hat{\alpha}+\hat{\beta}), & \Delta > \frac{PH_{tot}}{EA}, \\ -\frac{2}{3}\hat{\alpha}, & \Delta \le \frac{PH_{tot}}{EA}. \end{cases} \tag{55}$$

By definition, the function $\chi(d)$ is positive only for d in $[0, c_1/c_2)$. Since the values of d^+_{crit} and d^-_{crit} are defined and positive, one has $\hat{\gamma} > 0$ and $c_2 > 0$. Using the definitions of c_1, c_2 and $\hat{\gamma}$, we can show that $c_1/c_2 = d^\pm_{crit}$, where $+$ is associated with the first case and $-$ with the second case in Eq. (55). Since $d^\pm_{crit}$ are the critical damage levels for debonding or contact at the interface, as defined in Eqs. (43) and (44), damage states with $d \ge d^\pm_{crit}$, are excluded from the damage evolution of the adhesive interface.

Using (48), (42), (34) and (52), the driving force (46) takes the following form:

$$\hat{F}_d^{(-1)} = \hat{\gamma}\left(\frac{\Delta}{h} - \frac{P}{EA}\frac{H_{tot}}{h}\right)^2 \tag{56}$$

In the next Subsections, the two cases of a hard and a soft loading device are considered separately.

5.1. Hard loading device

We now consider the behavior of the adhesive joint under an imposed normal displacement Δ. For the sake of simplicity, we set $\hat{F}_d^{(-1)} := \mathcal{F}_{dH}$ for the hard device case. Substituting the force–displacement relation (53) into the driving force expression (56), the latter takes the form:

$$\mathcal{F}_{dH} = \frac{\hat{\gamma}}{(1+\chi(d))^2}\left(\frac{\Delta}{h}\right)^2. \tag{57}$$

Depending on Δ, different regimes may occur.

Proposition 5.1 (*Elastic Regime*). *Consider the joint under hard device loading. Let the imposed macroscopic normal displacement $\Delta(t)$ be a continuous function satisfying*

$$\Delta(t) \in (-\Delta_C, \Delta_T) \qquad \forall t \in [0,T], \tag{58}$$

where the elastic limits under contraction Δ_C and extension Δ_T are defined as

$$\Delta_C := h(1+c_1)\sqrt{-\frac{3\hat{k}_0}{2\hat{\alpha}}}, \qquad \Delta_T := h(1+c_1)\sqrt{-\frac{\hat{k}_0}{\hat{\alpha}+\hat{\beta}}}, \tag{59}$$

with $\hat{\alpha} < 0$, $\hat{\beta} < 0$ defined as in Section 2.1. Assume moreover that the initial damage is null, i.e. $d(0) = 0$.

Then the damage criterion is never activated for any $t \in [0,T]$, implying that the damage variable does not evolve:

$$d(t) = 0 \qquad \forall t \in [0,T]. \tag{60}$$

The corresponding macroscopic force–displacement response of the joint is linear elastic and is given by

$$P(t) = \frac{c_1}{(1+c_1)}\frac{EA}{H_{tot}}\Delta(t). \tag{61}$$

Proof. For $d = 0$, the damage driving force (57) simplifies to

$$\mathcal{F}_{dH} = \frac{\hat{\gamma}}{(1+c_1)^2}\left(\frac{\Delta}{h}\right)^2. \tag{62}$$

By definition, the two values $\Delta = -\Delta_C$ and $\Delta = \Delta_T$ are the unique solutions to the equation $\mathcal{F}_{dH} = \hat{k}_0$ for $\hat{\gamma} = -2\hat{\alpha}/3$ and $\hat{\gamma} = -(\hat{\alpha}+\hat{\beta})$, respectively. Therefore, the condition (58) is equivalent to $\mathcal{F}_{dH} < \hat{k}_0$. This implies that under the condition (58) the damage cannot evolve, i.e., $\dot{d} = 0$, and therefore $d(t) = 0$. Substituting $d = 0$ into the macroscopic equilibrium relation (53) gives the linear elastic response (61). □

Remark 2. Proposition 5.1 shows that the elastic regime is independent of the parameter $\hat{\eta}$ of the resistance function. Proposition 5.1 can be extended to states with non-vanishing initial damage. Indeed, assume that $d(0) = d_0 \in [0, d^\pm_{crit})$, where the plus sign applies under extension ($\Delta \ge 0$) and the minus sign under contraction ($\Delta < 0$). If the imposed normal displacement Δ satisfies the condition

$$\Delta(t) \in (-\Delta_C(d_0), \Delta_T(d_0)) \qquad \forall t \in [0,T],$$

where the elastic thresholds $\Delta_C(d_0)$ and $\Delta_T(d_0)$ are defined as

$$\Delta_C(d_0) := h(1+\chi(d_0))\sqrt{-\frac{3\hat{k}_0(1+\hat{\eta}d_0)}{2\hat{\alpha}}}, \tag{63}$$

$$\Delta_T(d_0) := h(1+\chi(d_0))\sqrt{-\frac{\hat{k}_0(1+\hat{\eta}d_0)}{\hat{\alpha}+\hat{\beta}}}, \tag{64}$$

then the damage criterion is never activated, and the damage variable remains constant and equal to the initial value, i.e. $d(t) = d_0\ \forall t \in [0,T]$. This occurs because the values $\Delta_C(d_0)$ and $\Delta_T(d_0)$ are the solutions of the damage activation condition

$$\tilde{f}(\mathcal{F}_{dH}(\Delta, d_0), d_0) = 0,$$

under the contraction and the extension of the joint, respectively. If the value of Δ falls within these values, the macroscopic force–displacement response of the joint is linear elastic and takes the form

$$P(t) = \frac{(c_1 - c_2 d_0)}{(1 + c_1 - c_2 d_0)} \frac{EA}{H_{tot}} \Delta(t), \tag{65}$$

characterized by a stiffness reduced by the presence of the term $c_2 d_0$, and depending on the initial damage. Since $d^{\pm}_{crit} = c_1/c_2$, this reduced stiffness in any elastic loading-unloading path is always well-defined for $d_0 \in [0, d^{\pm}_{crit})$.

Eq. (65) can be interpreted as the elastic unloading-reloading path law of the joint and is followed until damage activation. Once that the threshold for damage activation is exceeded, damage initiates in the adhesive, which further reduces the macroscopic stiffness of the joint. Depending on the material parameters and the initial damage level, the joint may exhibit a stable response or experience snap-back instability in the $\Delta - d$ plane, as shown in the following proposition.

Proposition 5.2 (*Damage Evolution and Snap-Back in Extension*). *Consider the joint under hard device loading and assume that the imposed macroscopic normal displacement $\Delta(t)$ is a monotonically increasing function of time. Let the initial damage be prescribed, $d(0) = d_0 \in [0, d^{+}_{crit})$, and assume that the elastic limit in extension, $\Delta_T(d_0)$, is exceeded.*

Then the damaging equilibrium path $\Delta - d$ under hard device loading is implicitly defined by the relation

$$\Delta(d) = h\sqrt{\frac{\hat{k}_0(1 + \hat{\eta} d)}{\hat{\gamma}}}\,(1 + c_1 - c_2 d), \qquad d \in [0, d^{+}_{crit}), \tag{66}$$

with $\hat{\gamma} = -(\hat{\alpha} + \hat{\beta})$. Let d_{sbH} denote the stationary point of the equilibrium path:

$$d_{sbH} := \frac{1}{3}\left(\frac{1 + c_1}{c_2} - \frac{2}{\hat{\eta}}\right). \tag{67}$$

Different situations may arise depending on the material parameters and initial damage.

A. *If $1 + c_1 - 3c_2 d_0 > 0$ and $c_1 < 1/2$ then the following three cases are possible.*
   - *(A.1) $\hat{\eta} \le \frac{2c_2}{1+c_1-3c_2 d_0}$ (brittle failure). The equilibrium path is monotonically decreasing (unstable) for all $d \in (d_0, d^{+}_{crit})$. At the end of the elastic regime, i.e., after reaching $\Delta = \Delta_T(d_0)$, the damage suddenly jumps from $d = d_0$ to d^{+}_{crit}, where failure occurs.*
   - *(A.2) $\frac{2c_2}{1+c_1-3c_2 d_0} < \hat{\eta} \le \frac{2c_2}{1-2c_1}$ (stable damage evolution followed by snap-back). The equilibrium path admits a local maximum at d_{sbH}. After the elastic regime, damage evolves from $d = d_0$ to $d = d_{sbH}$ following the equilibrium path (66). After reaching $\Delta = \Delta(d_{sbH})$, the damage suddenly jumps from $d = d_{sbH}$ to d^{+}_{crit}, where failure occurs.*
   - *(A.3) $\hat{\eta} > \frac{2c_2}{1-2c_1}$ (stable damage evolution). The equilibrium path is monotonically increasing in the interval (d_0, d^{+}_{crit}). After the elastic regime, damage evolves continuously along the equilibrium path (66) from $d = d_0$ until failure, occurring at $d = d^{+}_{crit}$.*

B. *If $1+c_1-3c_2 d_0 > 0$ and $c_1 = 1/2$, then the following cases are possible:*
   - *(B.1) $\hat{\eta} \le \frac{2c_2}{1+c_1-3c_2 d_0}$ (brittle failure), as in case A.1.*
   - *(B.2) $\hat{\eta} > \frac{2c_2}{1+c_1-3c_2 d_0}$ (stable damage evolution followed by snap-back), as in case A.2. In this case, $d_{sbH} < d^{+}_{crit}$ for every $\hat{\eta}$.*

C. *If $1+c_1-3c_2 d_0 > 0$ and $c_1 > 1/2$, then the following cases are possible:*
   - *(C.1) $0 < \hat{\eta} \le \frac{2c_2}{1+c_1-3c_2 d_0}$ (brittle failure), as in the case A.1.*
   - *(C.2) $\hat{\eta} > \frac{2c_2}{1+c_1-3c_2 d_0}$ (stable damage evolution followed by snap-back), as in the case A.2.*

D. *If $1 + c_1 - 3c_2 d_0 \le 0$ (brittle failure), then case A.1 occurs for any $\hat{\eta} > 0$.*

Proof. After damage initiation, the evolution of the adhesive is governed by the third case of the consistency conditions (47). From the expression of the damage driving force under hard device loading (57), the first condition $\tilde{f}(\mathcal{F}_{dH}, d) = 0$ yields the relation (66), which defines the damaging equilibrium path. Once $\Delta(d)$ is explicitly characterized, the second relation $\dot{\tilde{f}}(\mathcal{F}_{dH}, d) = 0$ is automatically satisfied.

By differentiating $\Delta(d)$ with respect to d, we obtain

$$\Delta'(d) = \frac{h}{2}\sqrt{\frac{\hat{k}_0}{\hat{\gamma}(1 + \hat{\eta} d)}}\Big(\hat{\eta}(1 + c_1 - 3c_2 d) - 2c_2\Big). \tag{68}$$

Imposing $\Delta'(d) = 0$ yields the unique critical point d_{sbH} defined in (67), which corresponds to a local maximum, since $c_2 > 0$. The stability of the system at damage initiation depends on the sign of $\Delta'(d_0)$. We now distinguish the different cases.

First, assume that $1 + c_1 - 3c_2 d_0 > 0$ and $c_1 < 1/2$, corresponding to case A.

- (*A.1*) If $0 < \hat{\eta} \le \frac{2c_2}{1+c_1-3c_2 d_0}$, then $d_{sbH} \le d_0$, implying that $\Delta'(d_0) \le 0$. This means that the system is in an unstable state at the end of the elastic regime. After increasing Δ, a snap-back occurs immediately: damage discontinuously increases from d_0 to $d = d^{+}_{crit}$ and the adhesive fails. Correspondingly, the force–displacement curve of the joint exhibits a sudden drop to $P = 0$.
- (*A.2*) If $\frac{2c_2}{1+c_1-3c_2 d_0} < \hat{\eta} \le \frac{2c_2}{1-2c_1}$, then $d_0 < d_{sbH} \le d^{+}_{crit}$, implying that $\Delta'(d_0) > 0$. After the end of the elastic regime, damage evolves along the ascending branch of the equilibrium path (66) starting from $d = d_0$ up to its local maximum $d = d_{sbH}$. At this point $\Delta'(d_{sbH}) = 0$ and further increments of Δ make the damage suddenly jumps from d_{sbH} to d^{+}_{crit}. The latter value corresponds to the total damage of the adhesive, and correspondingly the macroscopic force P drops to zero.
- (*A.3*) If $\hat{\eta} > \frac{2c_2}{1-2c_1}$, then $d^{+}_{crit} < d_{sbH}$, implying that $\Delta'(d) > 0$ for all $d \in [d_0, d^{+}_{crit})$. Damage evolves continuously along the equilibrium path from $d = d_0$ up to $d = d^{+}_{crit}$, the limit corresponding to full adhesive damage. The force–displacement response of the joint exhibits a smooth stiffness reduction until $P = 0$.

Next, assume that $1 + c_1 - 3c_2 d_0 > 0$ and $c_1 = 1/2$, corresponding to case B.

- (*B.1*) If $\hat{\eta} \le \frac{2c_2}{1+c_1-3c_2 d_0}$, then $d_{sbH} \le d_0$, implying that $\Delta'(d_0) \le 0$. As in case *A.1*, the system is unstable at the end of the elastic regime and brittle failure occurs immediately.
- (*B.2*) If $\hat{\eta} > \frac{2c_2}{1+c_1-3c_2 d_0}$, then $d_0 < d_{sbH} \le d^{+}_{crit}$, implying that $\Delta'(d_0) > 0$. Damage first evolves along the stable branch of the equilibrium path (66) from $d = d_0$ to $d = d_{sbH}$. At this point, $\Delta'(d_{sbH}) = 0$, and further increments of Δ lead to snap-back, with a sudden jump from d_{sbH} to d^{+}_{crit}.

Next, assume that $1 + c_1 - 3c_2 d_0 > 0$ and $c_1 > 1/2$, corresponding to case C.

- (*C.1*) If $0 < \hat{\eta} \le \frac{2c_2}{1+c_1-3c_2 d_0}$, then $d_{sbH} \le d_0$ for $\hat{\eta} \le \frac{2c_2}{1+c_1-3c_2 d_0}$, and case A.1 occurs, i.e. the behavior is brittle.
- (*C.2*) If $\hat{\eta} > \frac{2c_2}{1+c_1-3c_2 d_0}$, then d_{sbH} is always smaller that d^{+}_{crit} and case A.2 occurs, i.e. the damaging behavior is initially stable followed by snap-back.

Lastly, considering case D, if $1 + c_1 - 3c_2 d_0 \le 0$, then $d_{sbH} \le d_0$ for any positive value of the hardening parameter $\hat{\eta}$. Case A.1 always occurs, and the joint behavior is always brittle. □

Fig. 2 illustrates schematically the three subcases *A.1*, *A.2*, and *A.3* analyzed in case *A* of Proposition 5.2. On the left side, the equilibrium path in the $\Delta - d$ plane is shown. The green line corresponds to the elastic regime, the red line to stable damage evolution, and the magenta line to a non-equilibrium path characterized by a snap-back instability, indicated by an arrow. The right side shows the resulting macroscopic force–displacement response.

An analogous analysis can be performed under contraction, i.e., for $\Delta < 0$. In this case, the equilibrium path under hard device loading is again given by (66), with a minus sign in front of h to indicate contraction, and $\hat{\gamma} = -2\hat{\alpha}/3$. The existence of a snap-back is now governed by the condition $d_{sbH} \leq d^-_{crit}$. Since the damage value at which snap-back occurs, d_{sbH}, depends on $\hat{\gamma}$ via c_2, its value generally differs between the extension and contraction loading regimes. Since c_2 is typically larger under extension, snap-back is more likely to occur under extension than under contraction.

Finally, we note that the damage variable d is introduced as a geometrical density parameter that describes the microstructural state of the interface. Therefore, damage is considered here to be generated not only by the mechanical loading history, but also by defects arising from manufacturing processes, thermal loads or chemical processes. This implies that the initial value d_0 is not required to be reachable through a continuous damage evolution starting from an undamaged state. In particular, damage values with $d_0 > d_{sbH}$ are admissible as initial configurations, even though such states cannot be realized through a stable loading path under hard device conditions. We emphasize that the condition $\Delta'(d_0) > 0$ is necessary for the existence of a continuous post-elastic damage evolution, but not for the existence of a mechanical response. When this condition is violated, as in the case *A.1* of Proposition 5.2, the joint exhibits an elastic response up to the activation threshold, followed by an immediate failure.

5.2. Soft loading device

We now consider the response of the joint under soft device loading, where the macroscopic normal force P is prescribed and the displacement Δ is calculated using Eq. (53). Let us set $\hat{F}_d^{(-1)} := \mathcal{F}_{dS}$ for the soft device case. Substituting the force–displacement relation (53) into the driving force expression (56), we obtain:

$$\mathcal{F}_{dS} = \frac{\hat{\gamma} H_{tot}^2}{\chi^2(d) h^2} \left(\frac{P}{EA}\right)^2.$$

The occurrence of the snap-back is different from the hard device case. Here, the instability is observed in the P-d plane.

The elastic regime is identical under hard and soft device loading, so Proposition 5.1 and its extension to the case of non-vanishing initial damage, $d(0) = d_0 \in [0, d^{\pm}_{crit})$, still holds. The macroscopic force–displacement response of the joint is linear elastic and given again by (61). In terms of applied force, the elastic regime starting from vanishing damage corresponds to $P(t) \in (-P_C(d_0), P_T(d_0))$, where

$$P_C(d_0) := \frac{c_1 - c_2 d_0}{1 + c_1 - c_2 d_0} \frac{EA}{H_{tot}} \Delta_C(d_0),$$
$$P_T(d_0) := \frac{c_1 - c_2 d_0}{1 + c_1 - c_2 d_0} \frac{EA}{H_{tot}} \Delta_T(d_0). \tag{69}$$

Proposition 5.3 (*Damage Evolution and Snap-Back in Traction*). *Consider the joint under soft device loading, where the macroscopic normal force $P(t)$ is positive and prescribed. Let the initial damage be prescribed, $d(0) = d_0 \in [0, d^+_{crit})$, and assume that the applied force is greater than $P_T(d_0)$, the elastic limit corresponding to damage initiation.*

Then the damaging equilibrium path $P - d$ under soft device loading is implicitly defined by the relation

$$P(d) = \frac{EAh}{H_{tot}} \sqrt{\frac{\hat{k}_0(1 + \hat{\eta} d)}{\hat{\gamma}}} (c_1 - c_2 d), \qquad d \in [d_0, d^+_{crit}). \tag{70}$$

Let d_{sbS} denote the stationary point of the equilibrium path:

$$d_{sbS} = \frac{1}{3}\left(\frac{c_1}{c_2} - \frac{2}{\hat{\eta}}\right). \tag{71}$$

Different situations may arise depending on the material parameters and initial damage.

- *(A) If $c_1 - 3c_2 d_0 > 0$, then the following two cases are possible.*
  - *(A.1) $0 < \hat{\eta} \leq \frac{2c_2}{c_1 - 3c_2 d_0}$ (brittle failure). The equilibrium path is monotonically decreasing for all $d \in (d_0, d^+_{crit})$. At the end of the elastic regime, i.e., after reaching $P = P_T(d_0)$, the damage suddenly jumps from $d = d_0$ to d^+_{crit}, where failure occurs.*
  - *(A.2) $\hat{\eta} > \frac{2c_2}{c_1 - 3c_2 d_0}$ (stable damage evolution followed by snap-back). The equilibrium path admits a local maximum at d_{sbS}. After the elastic regime, damage evolves along the equilibrium path (70) from $d = d_0$ to $d = d_{sbS}$. After reaching $P = P(d_{sbS})$, the damage suddenly jumps from $d = d_{sbS}$ to d^+_{crit}, corresponding to the adhesive failure.*
- *(B) If $c_1 - 3c_2 d_0 \leq 0$, then case $A.1$ above occurs for any $\hat{\eta} > 0$.*

Proof. After damage initiation, the evolution follows the third case of the consistency condition in (47). Using the expression of the driving force under soft device loading, the condition $\tilde{f}(\mathcal{F}_{dS}, d) = 0$ yields the relation (70), which defines the damaging equilibrium path. The second condition $\dot{\tilde{f}}(\mathcal{F}_{dS}, d) = 0$ is then automatically satisfied.

By differentiating $P(d)$ with respect to d, we obtain

$$P'(d) = \frac{EAh}{H_{\text{tot}}} \sqrt{\frac{\hat{k}_0}{\hat{\gamma}}} \left(\frac{\hat{\eta}}{2\sqrt{1 + \hat{\eta} d}} (c_1 - c_2 d) - c_2 \sqrt{1 + \hat{\eta} d} \right). \tag{72}$$

Imposing $P'(d) = 0$ gives the critical point d_{sbS} defined in (71), corresponding to a local maximum since $c_2 > 0$. We now distinguish the different cases.

First, let us consider case A, with $c_1 - 3c_2 d_0 > 0$.

- $(A.1)$ If $0 < \hat{\eta} \leq \frac{2c_2}{c_1 - 3c_2 d_0}$, then $d_{sbS} \leq d_0$, implying that $P'(d_0) \leq 0$. The equilibrium path is not accessible from the initial state under soft device loading. Consequently, after increasing P, a brittle failure occurs immediately: damage discontinuously increases from d_0 to $d = d^+_{crit}$, the limit of full adhesive damage.
- $(A.2)$ If $\hat{\eta} > \frac{2c_2}{c_1 - 3c_2 d_0}$, then $d_{sbS} > d_0$, implying that $P'(d_0) > 0$. After the end of the elastic regime, damage evolves along the ascending branch of the equilibrium path (70) starting from $d = d_0$ up to its local maximum $d = d_{sbS}$. At this point $P'(d_{sbS}) = 0$ and further increments of P lead to instability, with a sudden jump from d_{sbS} to d^+_{crit}, corresponding to failure.

For case B, if $c_1 - 3c_2 d_0 \leq 0$, then $d_{sbS} \leq d_0$ for any positive value of the parameter $\hat{\eta} > 0$. Hence case *A.1* always occurs. The joint is always unstable at the end of the elastic regime, resulting in brittle failure. □

Comparison of (67) and (71) shows that $d_{sbS} < d_{sbH}$. Therefore, for the same material parameters c_1, c_2 and $\hat{\eta}$, a snap-back is more likely to occur under soft device loading than under hard device loading. In other words, the system may exhibit a snap-back in the $P - d$ plane under soft device loading even when the response in the $\Delta - d$ plane under hard device loading is a stable damage evolution along the equilibrium path (66).

Moreover, unlike the hard device case, a fully stable evolution up to failure analogous to the third case of Proposition 5.2 is impossible under soft device loading. This is because d_{sbS} is always less than d^+_{crit} for any $\hat{\eta}$. So, if $d_0 < d_{sbS}$, then the force $P(d)$ always reaches the local maximum, from which a snap-back occurs.

An analogous analysis can be performed under compression, i.e. for $P < 0$. In this case, the equilibrium path under soft device loading is

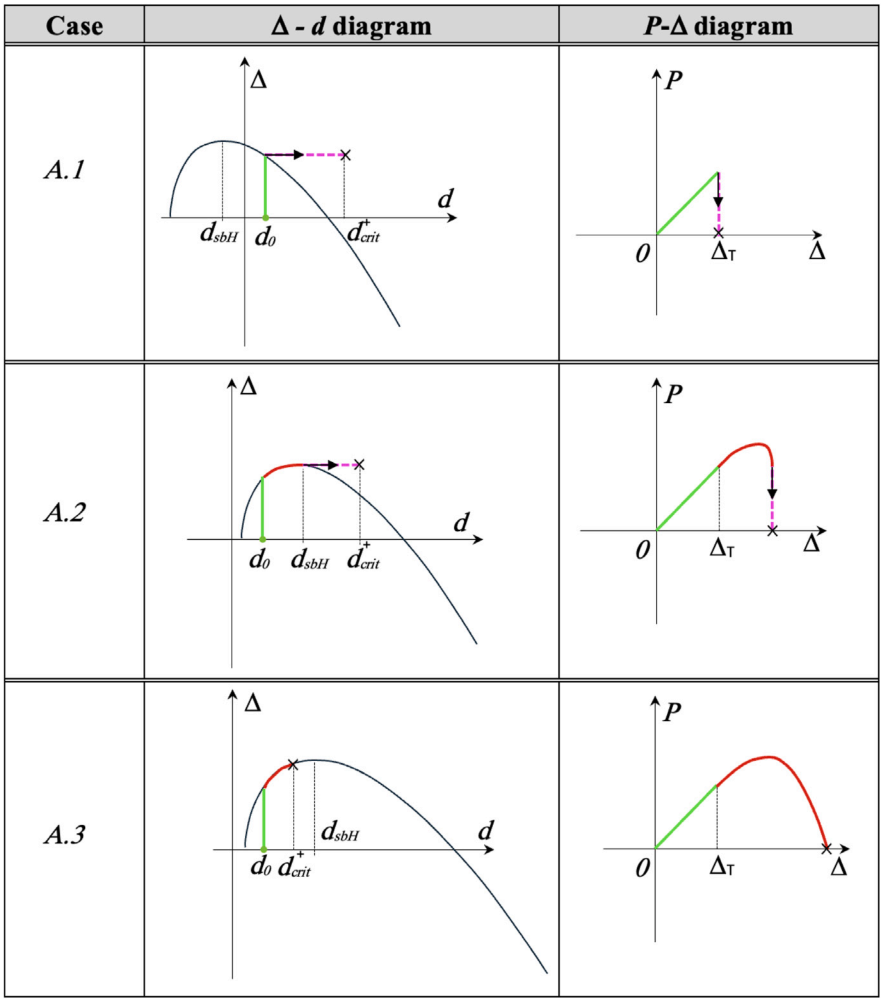

Fig. 2. Schematic representation of subcases *A.1*, *A.2*, and *A.3* of Proposition 5.2. Green denotes the elastic regime, red the stable damage evolution, and magenta the snap-back instability. Left: $\Delta - d$ equilibrium path. Right: macroscopic force–displacement response. Arrows indicated snap-back instability. The cross denotes complete damage. (For interpretation of the references to color in this figure legend, the reader is referred to the web version of this article.)

again given by (70), with a minus sign in front of EAh/H_{tot} to indicate compression, and $\hat{\gamma} = -2\hat{\alpha}/3$. The existence of a snap-back is now governed by the position of d_{sbS} relative to the initial damage, d_0, and the compressive failure limit, d^-_{crit}.

5.3. Numerical simulations

To investigate the nonlinear response of the adhesive butt joint, we implemented our theoretical results in MATLAB [49]. First, we show that our model can successfully reproduce experimental data [50]. Next, we apply the model to illustrate the stability conditions and snap-back phenomena discussed in Proposition 5.2.

5.3.1. Experimental validation and numerical results for the soft loading device

To assess the physical plausibility of the interface model, we compare its predictions with the experimental data for axially loaded adhesive butt joints reported by Adams and Coppendale in [50]. These authors analyzed butt joints composed of EN 25 steel adherents and BSL 308A film adhesive. The tests were conducted quasi-statically by recording the extensometer reading between increments of applied load. This experimental setup corresponds to a soft loading device. To compare with our simulations, we digitized the experimental stress–strain data from the published results using the web based software *WebPlotDigitizer* [51].

The geometrical and initial material properties of the adherents and the adhesive used in the simulation are listed in Table 1. The damage parameters $\hat{k}_0$ and $\hat{\eta}$ were chosen to match the nonlinear softening branch of the experimental tensile curve. The initial damage is set to zero, i.e., $d_0 = 0$.

In the left side of Fig. 3, the stress–strain response predicted by the model, represented by the continuous and dashed lines, is compared with the experimental data points, marked with crosses. The model exhibits excellent agreement with the experimental observations both in traction and compression. In tension, the model captures the transition from linear elasticity (green line) to the softening response (red line), and it reproduces the progressive stiffness degradation observed in the experiment. In compression, the model matches the experimental stiffness. However, the numerical prediction extends to significantly higher stress levels than the experimental data. This is consistent with the experimental procedure reported in [50], where it is reported that the specimens were first loaded in compression without reaching failure, to allow for subsequent testing in tension. The damage evolution is shown on the right side Fig. 3. The model predicts that at the maximum compressive stress of 340 MPa reached in the experiment, the damage variable reaches a value of $d \approx 0.04$. This indicates that, although the damage threshold was slightly exceeded, the resulting material degradation was minimal (4%). Our numerical prediction of the damage is consistent with the experimental procedure, in which the specimen was first loaded in compression to a stress of 340 MPa

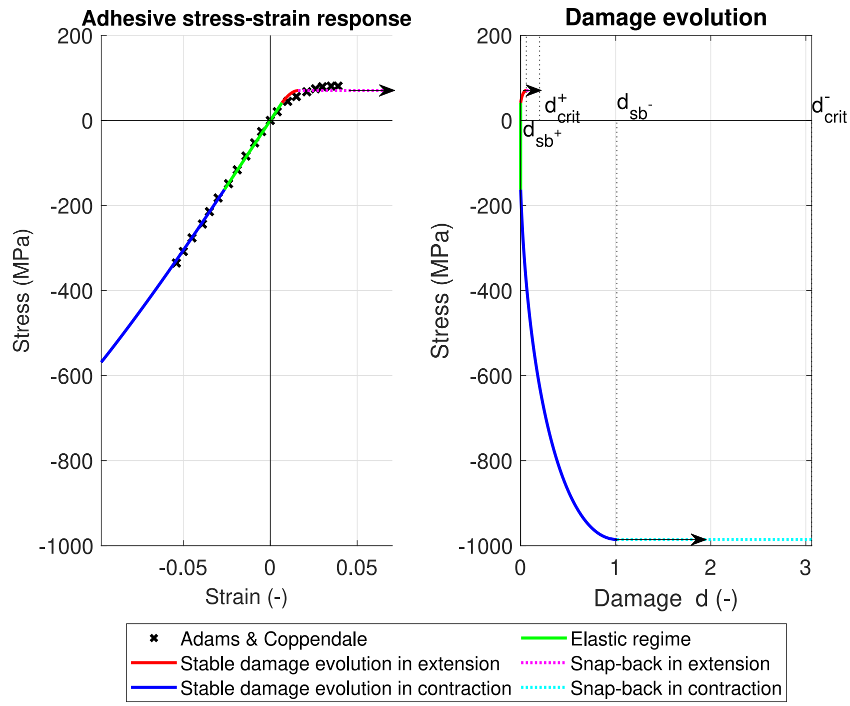

Fig. 3. Left: comparison of simulated stress–strain curves for a butt joint under soft loading device with experimental data for an adhesive butt joint (BSL308A) from Adams and Coppendale [50]. Right: damage evolution with applied stress, as predicted by the numerical model. Arrows indicate snap-back instabilities. (For interpretation of the references to color in this figure legend, the reader is referred to the web version of this article.)

Table 1
Geometrical and material parameters used in the numerical simulations.

	Quantity	Symbol	Value	Unit
Geometry	Total height	H_{tot}	24.50[a]	mm
	Adhesive's thickness	h	0.39[b]	mm
	Bonded section area	A	641[c]	mm^2
Adherents	Young's modulus	E	210[d]	GPa
	Poisson's ratio	ν	0.30[d]	–
Adhesive	Undamaged Young's modulus	$\hat{E}_0$	3.31[e]	GPa
	Undamaged Shear modulus	$\hat{\mu}_0$	1.20[e]	GPa
	Damage resistance	$\hat{k}_0$	0.70[f]	MPa
	Damage parameter	$\hat{\eta}$	See note[g]	–
	Damage parameter	$\hat{\alpha}$	−1510.34	MPa
	Damage parameter	$\hat{\beta}$	−13 875.02	MPa

[a] Gauge length, as reported in [50].
[b] Total adhesive thickness, as reported in [50].
[c] Calculated from reported inner (36 mm) and outer (46 mm) diameters [50].
[d] Assumed value for EN25 steel.
[e] Values reported in [52].
[f] Value chosen to give a good qualitative fit to the experimental data, cf. Section 5.3.2.
[g] Under soft loading device, value chosen for good qualitative fit: $\hat{\eta} = 80$ (Fig. 3), cf. Section 5.3.2. Under hard loading device, $\hat{\eta} = 0.4$ (Fig. 5), $\hat{\eta} = 4.0$ (Fig. 6), $\hat{\eta} = 40.0$ (Fig. 7).

and, since no apparent damage was caused by the compression test, the specimen was subsequently loaded to failure in tension [50].

Finally, note that, given the chosen geometrical and material parameters, the model predicts a stable damage evolution (red and blue curves) followed by snap-back (magenta and cyan lines), in both traction and compression.

5.3.2. Parameter assignment and robustness

The parameters of the interface model have different origins. The geometric parameters of the joint are taken from the experimental configuration [50]. The elasticity properties of the adherents are standard values for the considered materials. The undamaged elasticity constants of the adhesive, $\hat{E}_0$ and $\hat{\mu}_0$, are obtained from [52]. The damage parameters $\hat{\alpha}$ and $\hat{\beta}$ are computed from the micromechanical relations (12), and therefore they inherit the interpretation associated with the opening and closure of microcracks.

The remaining parameters of the interfacial damage law are the damage resistance $\hat{k}_0$ and the damage parameter $\hat{\eta}$. These parameters govern different aspects of the damage process. The parameter $\hat{k}_0$ represents the initial resistance to damage and therefore affects the onset of damage. The parameter $\hat{\eta}$ controls the damage evolution and the position of the stationary points of the equilibrium paths, $d^{\pm}_{sb}$. In the present application, these two parameters were calibrated by matching the nonlinear part of the tensile response of the experimental test, while keeping the other geometric and material parameters fixed.

A sensitivity analysis was carried out under soft loading conditions to assess the robustness of the predictions with respect to the calibrated values. Starting from the reference values listed in Table 1, $\hat{k}_0$ and $\hat{\eta}$ were varied independently by ±30%. Fig. 4 shows the resulting eight responses compared with the reference response.

The stress–strain response appears robust with respect to the considered variations of both $\hat{k}_0$ and $\hat{\eta}$ over the strain range covered by experimental data. Indeed, in this range all the perturbed curves remain close to the reference case and exhibit the same qualitative behavior. The same conclusion applies to the tensile part of the stress–damage response, where only minor variations are evident.

Large differences emerge in the compression part of the stress–damage response, even though the overall structure of the response is preserved in all cases. As expected from its role in the resistance function, the stable damage evolution branches becomes wider for larger values of $\hat{\eta}$. The stress plateau reached at snap-back is also sensitive to changes in both parameters, with larger values generally associated with higher plateau levels in absolute value.

The asterisks in Fig. 4 mark the stationary points $d^{\pm}_{sb}$ for the different sensitivity cases. The maximum relative variation with respect to the reference case is approximately 6.1% for d^{+}_{sb} and only 0.35% for d^{-}_{sb}. Overall, the results of the sensitivity analysis demonstrate that the main predictions of the model are robust with respect to moderate variations of the two calibrated parameters, $\hat{k}_0$ and $\hat{\eta}$.

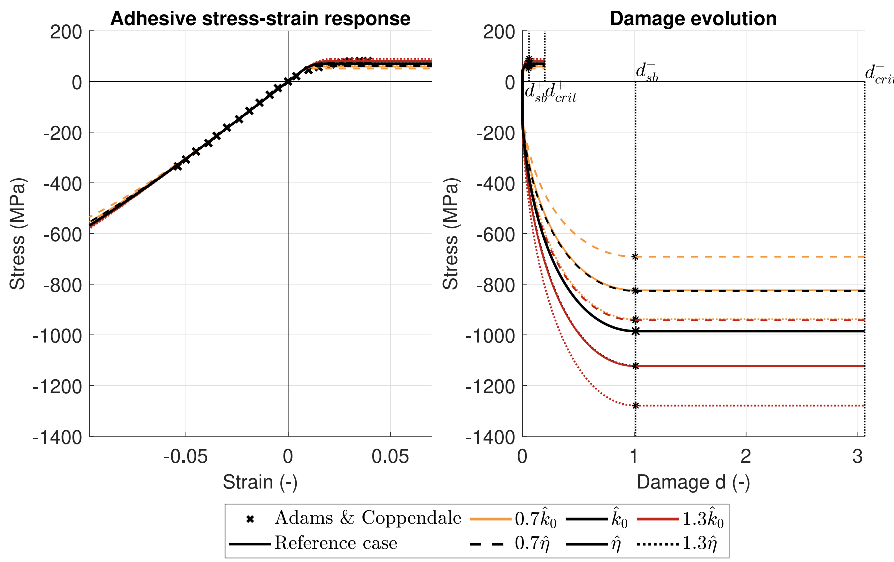

Fig. 4. Sensitivity analysis for the soft loading device. The different curves are obtained by varying $\hat{k}_0$ and $\hat{\eta}$ by ±30% around they reference values. The colors identify variations in $\hat{k}_0$, the line styles variations in $\hat{\eta}$ and the black continuous lines correspond to the reference case. Left: macroscopic stress–strain response compared with the data by Adams and Coppendale. Right: stress–damage response, with markers indicating the points $d_{sb}^{\pm}$. The vertical dotted line refer to the reference values of $d_{sb}^{\pm}$ and $d_{crit}^{\pm}$. (For interpretation of the references to color in this figure legend, the reader is referred to the web version of this article.)

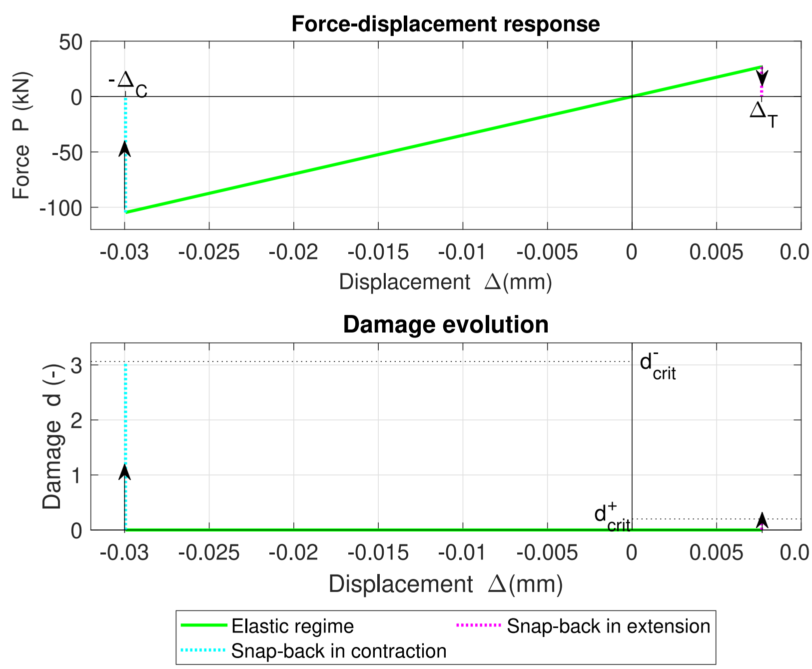

Fig. 5. Joint's response with $\hat{\eta} = 0.4$ under hard loading device: brittle under extension and brittle under contraction. Top: macroscopic force–displacement response. Bottom: damage evolution. Arrows denote snap-back in extension and contraction. (For interpretation of the references to color in this figure legend, the reader is referred to the web version of this article.)

5.3.3. Numerical results for the hard loading device

To investigate the stability conditions and snap-back phenomena predicted by Proposition 5.2 under the hard loading device, numerical simulations were performed by varying the parameter $\hat{\eta}$, while keeping the geometric and remaining material parameters fixed, as listed in Table 1. For those values, we find that the parameter c_1 is approximately 1.91. The corresponding values of the parameter c_2 are 0.62 and 9.54 for extension and contraction, respectively. These values explain why the conditions for snap-back differ between extension and contraction. Since $c_1 > 1/2$, we fall into case C of Proposition 5.2, so that only two regimes are possible, depending on $\hat{\eta}$: elastic behavior followed by snap-back (case $C.1$, corresponding to case $A.1$), and damage evolution followed by snap-back (case $C.2$, corresponding to case $A.2$). Three distinct cases were simulated, corresponding to the following values of $\hat{\eta}$: 0.4, 4.0 and 40.0.

The results of the simulations are presented in Figs. 5–7 in terms of the macroscopic force–displacement response of the joint. This representation is preferred over the adhesive stress–strain response because the snap-back is clearly visualized in the $P - \Delta$ plane as a vertical drop in the force at a fixed displacement. First, consider the case with $\hat{\eta} = 0.4$. With this low value, the joint exhibits a brittle behavior during both extension and contraction, as shown in Fig. 5. This corresponds to the case $A.1$ of Proposition 5.2, where the condition $d_{sbH} \leq 0 = d_0$ is satisfied. Thus, at the end of the elastic regime (green line), the

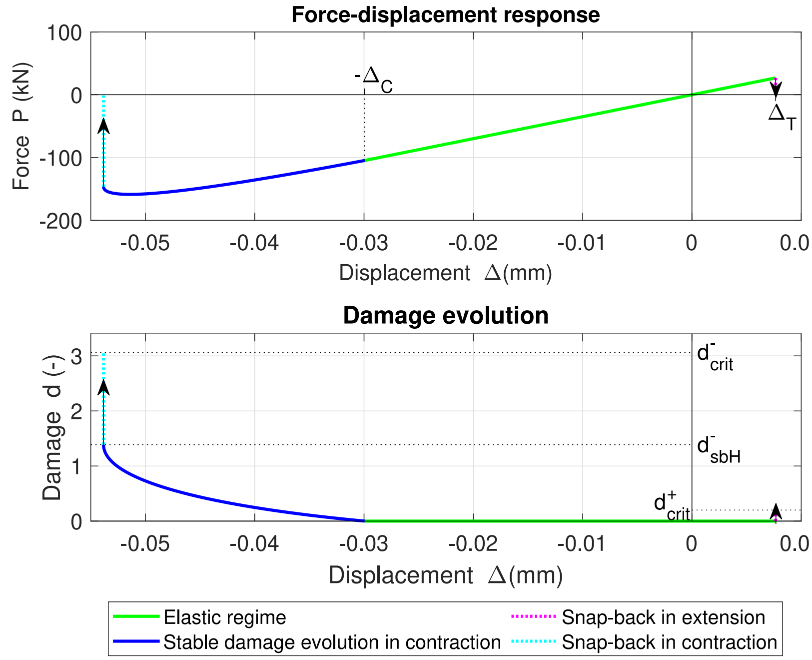

Fig. 6. Joint's response with $\hat{\eta} = 4.0$ under hard loading device: brittle under extension and stable damage evolution followed by snap-back under contraction. Top: macroscopic force–displacement response. Bottom: damage evolution. Arrows indicate snap-back. (For interpretation of the references to color in this figure legend, the reader is referred to the web version of this article.)

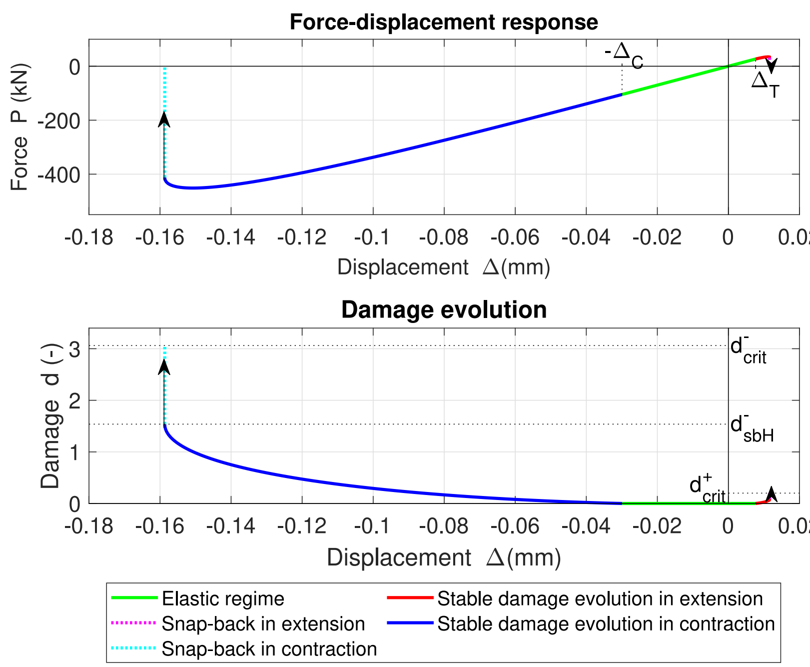

Fig. 7. Joint's response with $\hat{\eta} = 40.0$ under hard loading device: stable damage evolution followed by snap-back bith under extension and contraction. Top: macroscopic force–displacement response. Bottom: damage evolution. Arrows indicate snap-back. (For interpretation of the references to color in this figure legend, the reader is referred to the web version of this article.)

damage suddenly jumps from $d = 0$ to the failure threshold $d^{\pm}_{crit}$ (magenta line in extension, cyan line in contraction). Correspondingly, the force–displacement curve of the joint drops to zero force.

Fig. 6 illustrates an intermediate case with $\hat{\eta} = 4.0$. Here, the response is brittle in extension (magenta line), as in case $A.1$, but damage evolves in a stable way (blue curve) followed by snap-back (cyan line) in contraction, as in case $A.2$. This occurs because in extension the condition for the brittle regime is met, $d^{+}_{sbH} \leq 0$, while in contraction, the condition for stable initiation is satisfied, $d^{-}_{sbH} = 1.29 > 0$. This behavior is due to the different values taken by the parameter c_2 in traction and in compression, which in turn is related, via $\hat{\gamma}$, to the microcrack-induced asymmetry at the basis of the damage model.

Finally, for a sufficiently high hardening parameter, $\hat{\eta} = 40.0$, after the elastic regime (green line), the damage evolution is initially stable under both extension and contraction, as in case $A.2$. This behavior is shown in Fig. 7. The joint follows the stable branch of the equilibrium path (red curve in tension, blue in contraction) until the displacement reaches the local maximum $\Delta(d_{sbH})$. Beyond this point, equilibrium cannot be maintained under displacement control, the adhesive fails and the force drops to zero.

6. Conclusions

In this work, the mechanical behavior of thin adhesive layers exhibiting tension–compression asymmetry has been investigated by adopting a strain-based isotropic damage model with unilateral effects within a thermodynamically consistent framework.

A novel interface model, including the corresponding damage evolution, has been formally derived through the asymptotic expansions method. The resulting formulation is able to capture stiffness degradation under tensile loading together with partial stiffness recovery under compression, consistently reflecting the microcrack opening–closure mechanisms. This provides a clear link between the micromechanical interpretation of damage and the macroscopic response of bonded structures. From a modeling perspective, the proposed approach offers a consistent and physically grounded alternative to standard cohesive interface models, whose parameters are often only phenomenologically defined.

The range of validity of the proposed interface law is restricted to sufficiently thin adhesive layers, smooth and macroscopically homogeneous interfaces. For relatively thick adhesive layers, the zero-th order interface law may no longer be sufficient, and higher-order terms in the asymptotic expansion should be retained. Rough or heterogeneous interfaces, pronounced through-thickness stress or strain gradients, localized edge effects, or abrupt spatial variations along the interface may instead require an enrichment of the initial three-dimensional model. Such effects could be incorporated, for instance, by accounting explicitly for surface roughness, local thickness variations, or interfacial heterogeneities (see e.g. [37]), or by adopting generalized continuum theories, such as strain gradient or micropolar elasticity (see e.g. [53]).

The application to a uniaxial test on a butt joint has highlighted the relevance of unilateral effects in governing the global mechanical behavior. The numerical results show that the tension–compression asymmetry significantly influences both the evolution of damage and the force–displacement response, leading to markedly different behaviors under tensile and compressive regimes. In particular, the model reproduces distinct stiffness characteristics and activation thresholds for damage, which cannot be captured by classical symmetric formulations. Indeed, the analytical results established in Propositions 5.1 and 5.2 for a hard loading device and Proposition 5.3 for a soft loading device, clarify the qualitative properties of the solution, highlighting the conditions under which different mechanical global responses occur, namely elastic regime, damage evolutions with softening and snap-back instabilities in extension and contraction.

The validation presented in this work, although limited to a uniaxial butt joint configuration, was intended as a first controlled benchmark for assessing the consistency of the proposed interface formulation. This configuration was selected because it allows the effects of unilateral damage to be examined separately from additional complexities related to geometry, mixed-mode interaction, or non-proportional loading. In this setting, the model is able to highlight the role of tension–compression asymmetry in the activation of damage, the degradation or recovery of stiffness, and the occurrence of unstable post-peak responses. Nevertheless, broader validation is still required to evaluate the predictive capabilities of the model in more general applications. Future developments will therefore focus on mixed-mode loading conditions, more complex bonded joint geometries, and cyclic or non-proportional loading paths, where the coupling between normal and tangential displacement jumps is expected to play a significant role. The incorporation of rate-dependent effects, such as viscoelasticity, and a more detailed analysis of stability and post-critical behavior also represent important directions for further research.

CRediT authorship contribution statement

Michele Serpilli: Writing – review & editing, Writing – original draft, Validation, Supervision, Methodology, Investigation, Funding acquisition, Formal analysis, Conceptualization. **Raffaella Rizzoni:** Writing – review & editing, Writing – original draft, Visualization, Validation, Supervision, Software, Methodology, Investigation, Funding acquisition, Formal analysis, Data curation, Conceptualization. **Hélène Welemane:** Writing – review & editing, Writing – original draft, Validation, Supervision, Methodology, Investigation, Funding acquisition, Formal analysis, Conceptualization. **Frédéric Lebon:** Writing – review & editing, Validation, Supervision, Project administration, Methodology, Investigation, Funding acquisition, Conceptualization.

Declaration of competing interest

The authors declare the following financial interests/personal relationships which may be considered as potential competing interests: Michele Serpilli and Raffaella Rizzoni are currently serving as Guest Editors of the Special Issue entitled Multiscale asymptotic methods in solid mechanics. Given their role as Guest Editors, they had no involvement in the peer review of this article and had no access to information regarding its peer review. Full responsibility for the editorial process for this article was delegated to another journal editor. If there are other authors, they declare that they have no known competing financial interests or personal relationships that could have appeared to influence the work reported in this paper.

Acknowledgments

RR gratefully acknowledges the support of the project LESSGAS (CUP: B79J25000600005 - COR: 24519183). This research has been conducted according to the inspiring scientific principles of the Italian National Group for the Mathematical Physics (GNFM) of the National Institute for Advanced Mathematics (INdAM).

Data availability

The data used in this study were extracted from published figures in the literature (see [52]). No new experimental data were generated.

References

[1] M. Frémond, B. Nedjar, Damage in concrete: the unilateral phenomenon, Nucl. Eng. Des. 156 (1995) 323–335, http://dx.doi.org/10.1016/0029-5493(94)00970-A.

[2] J. Mazars, Y. Berthaud, S. Ramtani, The unilateral behaviour of damaged concrete, Eng. Fract. Mech. 35 (4–5) (1990) 629–635, http://dx.doi.org/10.1016/0013-7944(90)90145-7.

[3] Z. Wei, M. Zistl, S. Gerke, M. Brünig, Analysis of ductile damage and fracture under reverse loading, Int. J. Mech. Sci. 228 (2022) 107476, http://dx.doi.org/10.1016/j.ijmecsci.2022.107476.

[4] Z. Wei, S. Gerke, M. Brünig, Damage and fracture behavior under non-proportional biaxial reverse loading in ductile metals: experiments and material modeling, Int. J. Plast. 171 (2023) 103774, http://dx.doi.org/10.1016/j.ijplas.2023.103774.

[5] R. Liu, X.J. Wang, P.W. Chen, G. Kang, S.P. Zhu, Y.S. Guo, The role of tension-compression asymmetrical microcrack evolution in the ignition of polymer-bonded explosives under low-velocity impact, J. Appl. Phys. 129 (17) (2021) 175108, http://dx.doi.org/10.1063/5.0046011.

[6] L. Yang, Y. Yan, Y. Liu, Z. Ran, Microscopic failure mechanisms of fiber-reinforced polymer composites under transverse tension and compression, Compos. Sci. Technol. 72 (15) (2012) 1818–1825, http://dx.doi.org/10.1016/j.compscitech.2012.08.001.

[7] H. Zhang, K.T. Ramesh, E.S.C. Chin, A multi-axial constitutive model for metal matrix composites, J. Mech. Phys. Solids 56 (10) (2008) 2972–2983, http://dx.doi.org/10.1016/j.jmps.2008.07.001.

[8] J. Lemaitre, A continuous damage mechanics model for ductile fracture, J. Eng. Mater. Technol. 107 (1) (1985) 83–89, http://dx.doi.org/10.1115/1.3225775.

[9] J. Lemaitre, J.L. Chaboche, A. Benallal, R. Desmorat, Mécanique Des Matériaux Solides, third ed., Dunod, 2009.
[10] T. Park, B. Ahmed, G.Z. Voyiadjis, A review of continuum damage and plasticity in concrete: Part I – Theoretical framework, Int. J. Damage Mech. 31 (6) (2021) 901–954, http://dx.doi.org/10.1177/10567895211068174.
[11] C. Miehe, F. Welschinger, M. Hofacker, Thermodynamically consistent phase-field models of fracture: variational principles and multi-FIELD FE implementations, Internat. J. Numer. Methods Engrg. 83 (10) (2010) 1273–1311, http://dx.doi.org/10.1002/nme.2861.
[12] G. Lancioni, G. Royer-Carfagni, The variational approach to fracture mechanics. A practical application to the French Panthéon in Paris, J. Elasticity 95 (2009) 1–30, http://dx.doi.org/10.1007/s10659-009-9189-1.
[13] H. Amor, J.J. Marigo, C. Maurini, Regularized formulation of the variational brittle fracture with unilateral contact: numerical experiments, J. Mech. Phys. Solids 57 (8) (2009) 1209–1229, http://dx.doi.org/10.1016/j.jmps.2009.04.011.
[14] F. Vicentini, C. Zolesi, P. Carrara, C. Maurini, L. De Lorenzis, On the energy decomposition in variational phase-field models for brittle fracture under multi-axial stress states, Int. J. Fract. 247 (2024) 291–317, http://dx.doi.org/10.1007/s10704-024-00763-w.
[15] J. Zhang, J. Han, Q. Zhang, S. Reese, T. Brepols, Tension-compression asymmetry based on different energy decompositions within a gradient-extended two-surface damage-plasticity framework, Comput. Mech. 76 (2025) 1345–1379, http://dx.doi.org/10.1007/s00466-025-02652-y.
[16] I. Carol, K. Willam, Spurious energy dissipation/generation in stiffness recovery models for elastic degradation and damage, Int. J. Solids Struct. 33 (20–22) (1996) 2939–2957, http://dx.doi.org/10.1016/0020-7683(95)00254-5.
[17] J.-L. Chaboche, Damage induced anisotropy: On the diffculties associated with the active/passive unilateral condition, Int. J. Damage Mech. 1 (1992) 148–171, http://dx.doi.org/10.1177/105678959200100201.
[18] F. Cormery, H. Welemane, A critical review of some damage models with unilateral effect, Mech. Res. Commun. 29 (2002) 391–395, http://dx.doi.org/10.1016/S0093-6413(02)00262-8.
[19] H. Welemane, Une Modélisation Des Matériaux Microfissurés - Application Aux Roches Et Aux Bétons (thèse de doctorat), Université de Lille (France), 2002.
[20] H. Welemane, F. Cormery, An alternative 3D model for damage induced anisotropy and unilateral effect in microcracked materials, J. Phys. IV 105 (2003) 329–336, http://dx.doi.org/10.1051/jp4:20030204.
[21] H. Welemane, C. Goisdescu, Isotropic brittle damage and unilateral effect, C. R. Méc. 338 (2010) 271–276, http://dx.doi.org/10.1016/j.crme.2010.04.005.
[22] F. Cormery, H. Welemane, A stress-based macroscopic approach for microcracks unilateral effect, Comput. Mater. Sci. 47 (2010) 727–738, http://dx.doi.org/10.1016/j.commatsci.2009.10.016.
[23] G. Alfano, E. Sacco, Combining interface damage and friction in a cohesive-zone model, Internat. J. Numer. Methods Engrg. 68 (5) (2006) 542–582, http://dx.doi.org/10.1002/nme.1728.
[24] F. Cazes, A. Simatos, M. Coret, A. Combescure, A cohesive zone model which is energetically equivalent to a gradient-enhanced coupled damage-plasticity model, Eur. J. Mech. A Solids 29 (6) (2010) 976–989, http://dx.doi.org/10.1016/j.euromechsol.2009.11.003.
[25] A. Corigliano, M. Ricci, Rate-dependent interface models: formulation and numerical applications, Int. J. Solids Struct. 38 (4) (2001) 547–576, http://dx.doi.org/10.1016/S0020-7683(00)00088-3.
[26] Y.R. Kim, Cohesive zone model to predict fracture in bituminous materials and asphaltic pavements: state-of-the-art review, Int. J. Pavement Eng. 12 (4) (2011) 343–356, http://dx.doi.org/10.1080/10298436.2011.575138.
[27] Q. Xu, Z. Lu, An elastic–plastic cohesive zone model for metal–ceramic interfaces at finite deformations, Int. J. Plast. 41 (2013) 147–164, http://dx.doi.org/10.1016/j.ijplas.2012.09.008.
[28] L. Nazarenko, H. Stolarski, H. Altenbach, A statistical interphase damage model of random particulate composites, Int. J. Plast. 116 (2019) 118–142, http://dx.doi.org/10.1016/j.ijplas.2018.12.011.
[29] F. Lebon, R. Rizzoni, Asymptotic analysis of a thin interface: the case involving similar rigidity, Internat. J. Engrg. Sci. 48 (5) (2010) 473–486, http://dx.doi.org/10.1016/j.ijengsci.2009.12.001.
[30] F. Lebon, R. Rizzoni, Asymptotic behavior of a hard thin linear elastic interphase: An energy approach, Int. J. Solids Struct. 48 (3–4) (2011) 441–449, http://dx.doi.org/10.1016/j.ijsolstr.2010.10.006.
[31] R. Rizzoni, S. Dumont, F. Lebon, E. Sacco, Higher order model for soft and hard elastic interfaces, Int. J. Solids Struct. 51 (23–24) (2014) 4137–4148, http://dx.doi.org/10.1016/j.ijsolstr.2014.08.005.
[32] M. Serpilli, S. Lenci, An overview of different asymptotic models for anisotropic three-layer plates with soft adhesive, Int. J. Solids Struct. 81 (2016) 130–140, http://dx.doi.org/10.1016/j.ijsolstr.2015.11.020.
[33] F. Krasucki, A. Münch, Y. Ousset, Mathematical analysis of nonlinear bonded joint models, Math. Models Methods Appl. Sci. 14 (04) (2004) 535–556, http://dx.doi.org/10.1142/S0218202504003349.
[34] R. Rizzoni, S. Dumont, F. Lebon, On Saint Venant–Kirchhoff imperfect interfaces, Int. J. Non-Linear Mech. 89 (2017) 101–115, http://dx.doi.org/10.1016/j.ijnonlinmec.2016.12.002.
[35] M.L. Raffa, F. Lebon, G. Vairo, Normal and tangential stiffnesses of rough surfaces in contact via an imperfect interface model, Int. J. Solids Struct. 87 (2016) 245–253, http://dx.doi.org/10.1016/j.ijsolstr.2016.01.025.
[36] E. Bonetti, G. Bonfanti, F. Lebon, R. Rizzoni, A model of imperfect interface with damage, Meccanica 52 (2017) 1911–1922, http://dx.doi.org/10.1007/s11012-016-0520-1.
[37] M.L. Raffa, F. Lebon, R. Rizzoni, A micromechanical model of a hard interface with micro-cracking damage, Int. J. Mech. Sci. 216 (2022) 106974, http://dx.doi.org/10.1016/j.ijmecsci.2021.106974.
[38] S. Dumont, F. Lebon, M.L. Raffa, R. Rizzoni, H. Welemane, Multiscale modeling of imperfect interfaces and applications, in: Computational Methods for Solids and Fluids - Multiscale Analysis, Probability Aspects and Model Reduction, Springer, pp. 81–122, http://dx.doi.org/10.1007/978-3-319-27996-1.
[39] M. Serpilli, R. Rizzoni, F. Lebon, Predictive asymptotic models of damage evolution in thin adhesives with tension–compression asymmetry, Internat. J. Engrg. Sci. 217 (2025) 104384, http://dx.doi.org/10.1016/j.ijengsci.2025.104384.
[40] S. Dumont, M. Serpilli, R. Rizzoni, F.C. Lebon, Numerical validation of multiphysic imperfect interfaces models, Front. Mater. 7 (2020) 158, http://dx.doi.org/10.3389/fmats.2020.00158.
[41] M. Serpilli, R. Rizzoni, F. Lebon, S. Dumont, An asymptotic derivation of a general imperfect interface law for linear multiphysics composites, Int. J. Solids Struct. 180 (2019) 97–107, http://dx.doi.org/10.1016/j.ijsolstr.2019.07.014.
[42] H. Welemane, F. Cormery, Some remarks on the damage unilateral effect modelling for microcracked materials, Int. J. Damage Mech. 11 (1) 65–86, http://dx.doi.org/10.1106/105678902022260.
[43] D. Krajcinovic, Damage mechanics, Mech. Mater. 8 (2–3) (1989) 117–197, http://dx.doi.org/10.1016/0167-6636(89)90011-2.
[44] S. Andrieux, Y. Bamberger, J.J. Marigo, Un modèle de matériau microfissuré pour les roches et les bétons, J. Méc. Théor. Appl. 5 (3) (1986) 471–513.
[45] V. Pensée, D. Kondo, L. Dormieux, Micromechanical analysis of anisotropic damage in brittle materials, J. Eng. Mech. 128 (8) (2002) 889–897, http://dx.doi.org/10.1061/(ASCE)0733-9399(2002)128:8(889).
[46] J.J. Marigo, Formulation d'une loi d'endommagement d'un matériau élastique, C.R. Acad. Sci. Paris Sér. II (19) (1981) 33–36.
[47] D. Kondo, H. Welemane, F. Cormery, Basic concepts and models in continuum damage mechanics, Rev. Eur. Génie Civ. 11 (2007) 927–943, http://dx.doi.org/10.3166/regc.11.927-943.
[48] P.G. Ciarlet, Mathematical Elasticity. Theory of Plates, in: Series Studies in Mathematics and its Applications, vol. II, North-Holland, 1997.
[49] MATLAB Version: 24.1.0.2578822 (R2024a), The MathWorks Inc., Natick, Massachusetts, 2024.
[50] R.D. Adams, J. Coppendale, The stress-strain behaviour of axially-loaded butt joints, J. Adhes. 10 (1) (1979) 49–62, http://dx.doi.org/10.1080/00218467908544611.
[51] A. Rohatgi, WebPlotDigitizer, version 4.8, 2024, https://automeris.io/WebPlotDigitizer.
[52] R.D. Adams, J. Coppendale, Measurement of the elastic moduli of structural adhesives by a resonant bar technique, J. Mech. Eng. Sci. 18 (3) (1976) 149–158, http://dx.doi.org/10.1243/JMES_JOUR_1976_018_025_02.
[53] M. Serpilli, R. Rizzoni, F. Lebon, S. Dumont, Hard interfaces with microstructure: The cases of strain gradient elasticity and micropolar elasticity, Philos. Trans. A Math. Phys. Eng. Sci. 382 (2277) (2024) 20230308, http://dx.doi.org/10.1098/rsta.2023.0308.